Simulation Algorithms for Absorbing Receivers in Diffusion-Based Molecular Communication Systems: An *A Priori* Approach

Yiran Wang
U5639810

Supervised by Dr. Nan Yang

April 2020

A thesis submitted in part fulfilment of the degree of

Master of Philosophy in Engineering
The Department of Engineering
Australian National University

This thesis contains no material which has been accepted for the award of any other degree or diploma in any university. To the best of the author's knowledge, it contains no material previously published or written by another person, except where due reference is made in the text.

Yiran Wang
1 April 2020

Acknowledgement

Firstly, I would like to express my sincere gratitude to my supervisor Dr. Nan Yang for the continuous support during my MPhil study and related research, and for his patience, motivation, and immense knowledge.

I would also like to present my sincere appreciation to Dr. Adam Noel, my overseas co-supervisor, for his time and efforts on continuously providing precious comments on my project.

I would like to thank Assoc. Prof Xiangyun Zhou, my second supervisor, for the insightful advice and encouragement.

Completing this work would have been all the more difficult were it not for the support and friendship provided by the members of the Communications group in Research School of Engineering at ANU.

Finally, my study would not have been completed without all the love and help from my family, especially my dear parents. Thank you for bearing me in my ups and downs.

List of Publications

Journal Paper:

J1 **Y. Wang**, A. Noel, and N. Yang, "A novel *a priori* simulation algorithm for absorbing receivers in diffusion-based molecular communication systems," *IEEE Trans. Nanobiosci.*, vol. 18, no. 3, pp. 437-447, July 2019.

Conference Paper:

C1 **Y. Wang**, A. Noel, and N. Yang, "A new simulation algorithm for absorbing receivers in molecular communication," in *Proc. 2018 IEEE SECON,* Hong Kong, China, June 2018, pp. 1–4.

C2 Y. Fang, A. Noel, **Y. Wang**, and N. Yang, "Simplified cooperative detection for multi-receiver molecular communication," in *Proc. 2017 IEEE ITW,* Kaohsiung, Taiwan (ROC), Nov. 2017, pp. 329–333.

Abstract

Molecular Communication (MC) has emerged as a cutting edge technique for exchanging and conveying information among nano-devices in very small dimensions or specific environments, such as water, tunnels, and human bodies. It is worthwhile noting that existing simulation algorithms for diffusion-based MC systems incur high computational complexity when simulating the absorption of molecules at receiver(s). Specifically, the existing algorithms require a very small simulation time step length to accurately model the absorption, leading to a long simulation run time. Against this background, this thesis aims to reduce the computational complexity for the simulation of absorption at receiver(s) in a diffusion-based MC system.

In Chapter 3, the system models of the investigated problem are introduced. To be specific, the MC system with both a single absorbing receiver and that with multiple absorbing receivers are considered. The analytical reaction probabilities of molecules with absorbing receiver(s) are discussed. Furthermore, the intra-step absorption probabilities used in algorithms for simulating absorbing receiver(s) are presented.

In Chapter 4, existing simulation algorithms for absorbing receiver(s) in diffusion-based MC systems are carefully examined and the similarities and differences among algorithms are discussed. To quickly predict the simulation accuracy of an existing algorithm, the refined Monte Carlo (RMC) algorithm, a prediction expression is proposed as a function of the simulation time step length and system parameters. After discovering that the RMC algorithm enables accurate simulation for a relatively small simulation time step length only, a novel *a priori* Monte Carlo (APMC) algorithm is proposed to accurately simulate the molecules absorbed at spherical absorbing receiver(s) with low computational complexity for relatively large simulation time step lengths. Moreover, by analyzing the computational complexity of the APMC algorithm and the RMC algorithm, a likelihood threshold is proposed to reduce the computational complexity for both algorithms.

In Chapter 5, numerical results are shown to evaluate the aforementioned simulation algorithms. It is obvious from the results that using the prediction expression for the RMC algorithm, we can characterize the accuracy of the simulation results of the

RMC algorithm without running it, which facilitates the selection of simulation time step length for a given system. It is also demonstrated that the APMC algorithm effectively overcomes the shortcoming of the existing algorithms. It is further shown that after applying an appropriate likelihood threshold to the APMC algorithm and the RMC algorithm, the computational complexity is significantly saved while only an extremely small loss in accuracy is caused.

Contents

List of Figures

Chapter 1

Introduction

1.1 Background

For years, the innovation and advancement of communication and information systems have profoundly promoted the development of human society and civilization. Communication using electromagnetic waves is the traditional solution for conveying messages. However, this solution may not be practically feasible for nanoscale communication. Over the recent years, nanotechnologies have inspired new solutions to tackling the nanoscale communication problem. While a single bio-nanomachine can perform simple tasks such as sensing and performing basic motion, the techniques for bio-nanomachines to communicate and cooperate can significantly expand their capabilities.

Traditional communication technologies using electromagnetic waves have great difficulties to meet the requirements of nanoscale communication networks. Indeed, there are specific application areas where using electromagnetic waves is not feasible, for example, target drug delivery and water quality monitor applications. At the nano-level, a novel and practically feasible communication paradigm requires not only information and communication technologies, but also an interdisciplinary approach. Against this background, molecular communication (MC) has been acknowledged as a new paradigm for nanoscale communication since it allows bio-nanomachines to exchange and convey information based on the physical and chemical properties of molecules within the environment.

The area of MC was pioneered by Suda *et al.* in 2005 [7], which aimed at building the networks where bio-nanomachines can facilitate in communicating with each others. The initial efforts from these pioneers have pointed out some fundamental research activities in MC, including exploration of experimental and theoretical system models, identification of potential applications, and identification of future outlook in this field [8].

In MC, information is delivered via the propagation of molecules. One of the various types of propagation is diffusion, where the movements of molecules are modeled by Brownian motion. Diffusion-based MC focuses on building effective communication channels among bio-nanomachines within environments where the propagation of molecules depends on diffusion dynamics. In the literature of MC, simulations have served as an effective method for validating novel system models and evaluating the achievable performance of newly designed transmission strategies. Despite such importance, for diffusion-based MC, it has been noticed that the existing simulation algorithms are inadequate to accurately simulate molecule behaviors in the MC systems with absorbing receiver(s). This motivates the research presented in this thesis.

1.2 Thesis Overview

1.2.1 Contributions

The contributions of this MPhil thesis are summarized as follows:

1. A new algorithm, i.e., the *a priori* Monte Carlo (APMC) algorithm has been proposed for MC simulations with a relatively large simulation time step. The advantages of the APMC algorithm are:

   (a) For the case of a single perfectly absorbing receiver, it has been shown that by using the APMC algorithm, the fraction of molecules absorbed by the receiver precisely matches the corresponding analytical result when the average diffusion step length of molecules is relatively larger than the radius of the perfectly absorbing receiver.

   (b) For the case of two perfectly absorbing receivers, it has been shown that by using the APMC algorithm, the fraction of molecules absorbed by each of the receiver approaches the corresponding asymptotic analytical value when the total system transmission time grows large.

   It has been noticed that the advantages of the APMC algorithm in both cases cannot be achieved by the existing algorithms, such as those in [5, 6, 9].

2. Polynomial fitting expressions have been proposed to predict the accuracy of an existing algorithm introduced in [5], the refined Monte Carlo (RMC) algorithm, for the case of a single perfectly absorbing receiver. Aided by

numerical results, it has been demonstrated that the third order polynomial fitting expression is relatively accurate for prediction. With this expression, the accuracy of the RMC algorithm can be characterized without actually running it.

3. The computational complexity has been investigated for both the RMC algorithm and the APMC algorithm. Specifically, the MATLAB run times of both algorithms and the trade-off between simulation accuracy and computational complexity for both algorithms have been explored, based on which a likelihood threshold for the absorption probability has been proposed to save computation time. It has been defined that molecule absorption for the RMC algorithm and the APMC algorithm is possible if and only if the calculated absorption likelihood in the simulation is higher than the likelihood threshold. Aided by numerical results, it has been shown that applying a likelihood threshold can reduce as much as 20% of the total number of generated random variables in simulation with an extremely small loss in simulation accuracy.

1.2.2 Thesis organization

The organization of the thesis is as follows: Chapter 2 presents a review on related work on the research topic. The system environment of our investigated problem is introduced in Chapter 3. Existing simulation algorithms and our newly proposed algorithm for absorbing receiver(s) in diffusion-based MC systems are presented in detail in Chapter 4, where the similarities and differences among algorithms are also discussed. Chapter 5 shows the numerical results and discussions of simulation algorithms. Finally, the conclusion and future work are presented in Chapter 6.

Chapter 2

Literature Review

2.1 Overview

MC describes how information is exchanged using nano-scale particles, which is one of the most common ways of communication among biological entities [1]. Unlike electromagnetic wave-enabled communication, MC delivers information based on physical and chemical properties of molecules within the communication environment. Biological examples of MC include chemotactic signaling [10], calcium signaling [11], quorum sensing [12], bacterial migration [13], hormonal signaling [14], and neuronal signaling [15]. Compared to electromagnetic wave-enabled communication, the propagation speed of MC is extremely slow, the received signal in MC is rather unpredictable, and the transmission scale of MC is relatively limited [16]. On the other hand, MC offers some significant advantages such as low energy consumption, bio-compatibility, and the ability to communicate in the aqueous medium. Thus, MC has great potentials to transmit information that cannot be transmitted using the traditional electromagnetic wave-enabled communication technologies within the nanoscale environment.

As a communication system, the MC system has a layered architecture. This architecture is similar to the traditional one which is referred to as the Open System Interconnection model. A simple illustration of the information flow in an MC network is shown in Fig. 2.1. The MC architecture sends messages via information sources to the desired destinations and consists of five layers (from up to down): Application layer, transport layer, network layer, link layer and physical layer[17].

The physical layer, which electronic engineers are most concerned about, contains a signaling sublayer and a bio-nanomachine sublayer. The signaling sublayer is based on the Shannon's model of communication [18]. Basic components in this sublayer are messages, information sources and destinations, transmitters and receivers, communication channels, molecule storages and noise sources. It aims to build the

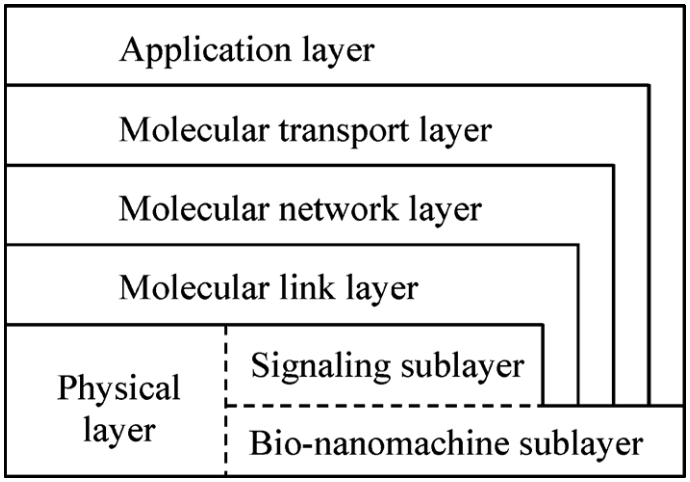

Figure 2.1: A layered architecture for MC networks [1, Chapter 4].

communication channels between bio-nanomachines. The bio-nanomachine sublayer explores the physical features of the bio-nanomachines required by upper layers and provides appropriately modified bio-materials to support the functionalities of the signaling sublayer. The signaling sublayer provides functionalities of signal modulation, demodulation, transmission and reception, propagation, and relay [2]. Detailed functionalities of each communication layer in MC networks can be further found in [17, Table I].

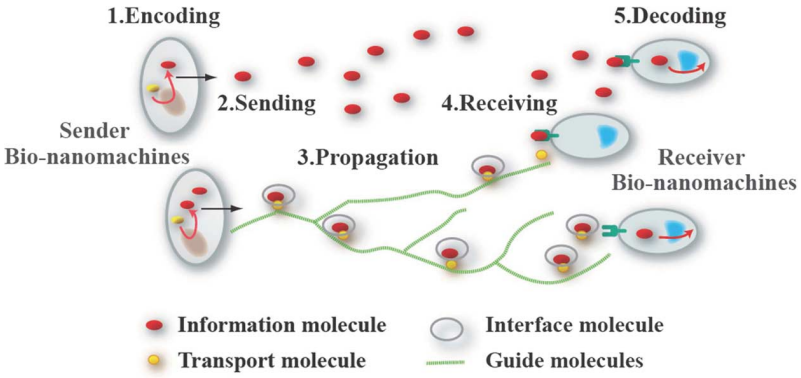

Figure 2.2: A typical model of MC system [1].

In a typical MC system, there are four major components: Transmitter(s), receiver(s), molecules, and a propagation environment where information-carrying molecules wander around, as shown in Fig. 2.2. There are five phases in a general process of MC, namely, modulation, transmission, propagation, reception and demodulation. The intended information is first encoded into the features of information-carrying molecules. Then, the transmitter in the system releases information-carrying molecules into the environment. Following this, molecules propagate within the environment and some of them are captured by the receivers. The properties of the

captured molecules can then be decoded to recover the carried information.

Information in MC is represented by the physical and chemical properties of molecules, such as the number of molecules, the structure of molecules, and the release timing of molecules. A basic example of modulation in MC is ON-OFF keying, which is the simplest amplitude-shift keying modulation from traditional communication and also a widely applied modulation scheme in MC. For ON-OFF keying in MC systems, the transmission time interval is set as a constant value. A group of molecules are released at the beginning of a transmission interval to represent the bit "1", while no molecule is released at all to express the bit "0".

The different modes where molecules propagate within the environment are named as propagation schemes. Propagation schemes in MC include passive propagation schemes, for example, pure random walk [19] and random walk with a drift [20, 21], and active propagation schemes, which are usually based on motor and filament proteins guiding and moving the information-carrying molecules [22, 23].

Moreover, there are two major types of receivers, namely, passive and active receivers [24]. While passive ones simply count the number of molecules that are within their visions, active receivers bind information-carrying molecules using receptors on their surfaces. Furthermore, active receivers include irreversible perfectly absorbing receivers and reversible absorbing receivers. The former receivers permanently remove all molecules that come into contact with the receiver boundary while the latter receivers may release molecules back to the environment at some time after binding or may react with the molecules on or inside their surfaces and produce new molecules.

Notably, the development of MC is envisioned to support various applications. Medical treatment, biological engineering, and environment monitoring are some promising areas that MC may help to advance. For example, MC may improve the quality of monitoring medical conditions and perform targeted drug delivery and other therapies [25, 26]. MC may also assist on analyzing biological tissues and organs [27, 28] and building interfaces between biological entities and electrical devices [29]. Furthermore, for agricultural industry, MC has the ability to monitor water or soil conditions and to identify the location of a contamination source. Overall, the development of MC is of particular importance for any application that may be benefited from nanoscale communication.

2.2 Modulation Schemes

In MC, information is usually represented by modulating on one or a combination of the following properties of molecules [30, 31, 32, 33, 34, 35, 36]:

1. Quantity of particles (Concentration Shift Keying): Information is encoded in the number or the concentration of information particles released [30, 31, 32], as depicted in Fig. 2.3. For example, in ON-OFF keying, a group of molecules are released at the beginning of a transmission interval to represent the bit "1" while no molecule is released at all in order to express the bit "0". If the receiver detects a number of molecules at the end during the current transmission interval and this number is higher than the specified decision quantity threshold, it can decide that the bit "1" was sent by the transmitter. Otherwise, it can decide that the bit "0" was sent by the transmitter.

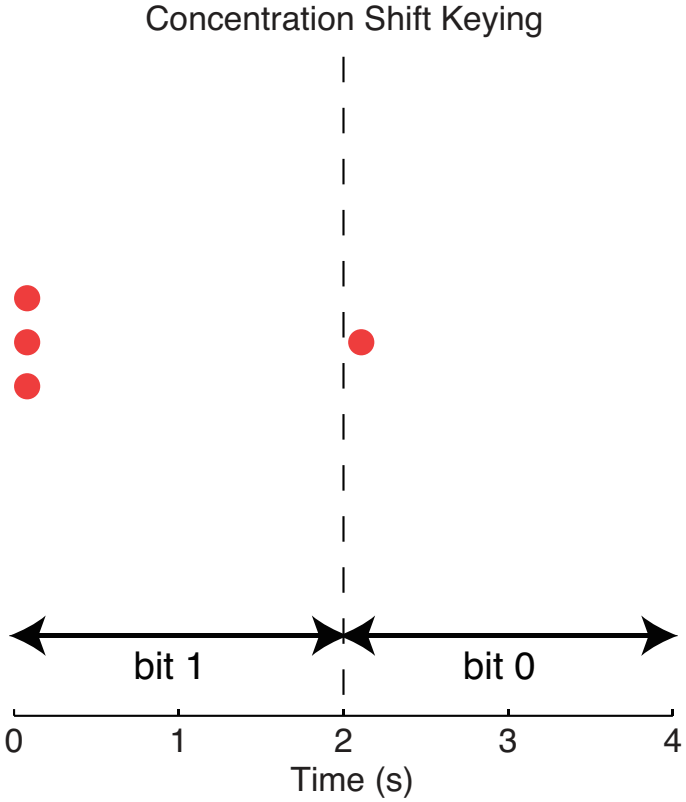

Figure 2.3: An example of modulating on the quantity of molecules in MC [2]. In this example, during time $t = [0, 2)$ s, the transmitter releases molecule(s) for the first bit of information and during time $t = [2, 4)$ s, the transmitter releases molecule(s) for the second bit of information. In this example, the transmitter releases three molecules (represented by red dots) to express the bit "1" for the first bit and releases one molecule to express the bit "0" for the second bit.

2. Structure of particles (Molecular Type Shift Keying): Information is encoded in the structure of released information particles [31, 32, 35, 36], as depicted in Fig. 2.4. For example, two types of molecules that have distinguishable structures, type-A and type-B, can be used to encode one bit of information. Type-A molecules can represent the bit "1" and type-B molecules can represent the bit "0". If type-A molecules are detected by the receiver during the current transmission interval, the receiver can decide that the bit "1" was sent by the transmitter. Otherwise, the receiver can decide that the bit "0" was sent by the transmitter.

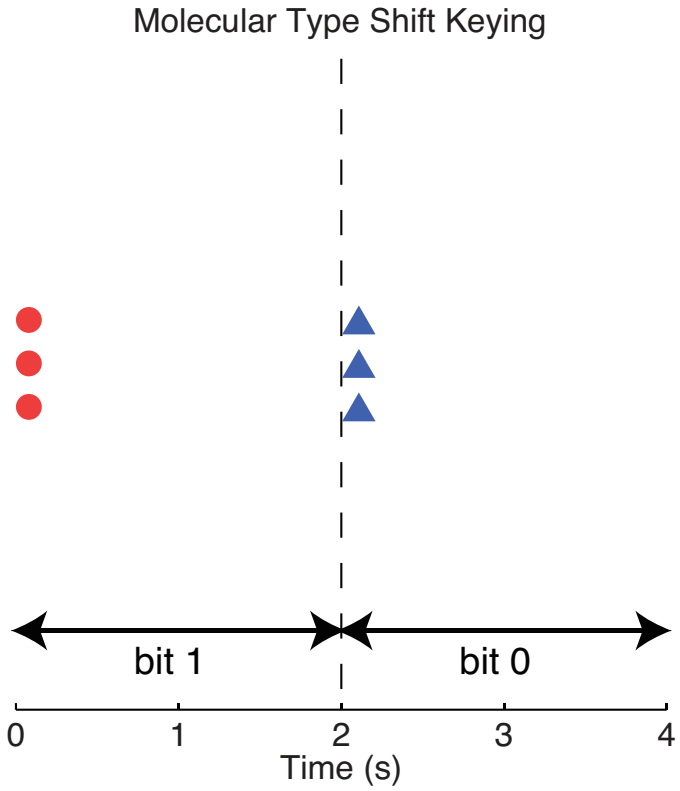

Figure 2.4: An example of modulating on the structure of molecules in MC [2]. In this example, during time $t = [0, 2)$ s, the transmitter releases molecule(s) for the first bit of information and during time $t = [2, 4)$ s, the transmitter releases molecule(s) for the second bit of information. In this example, the transmitter releases three type-A molecules (represented by red dots) to express the bit "1" for the first bit and releases three type-B molecules (represented by blue triangles) to express the bit "0" for the second bit.

3. Timing of release (Release Time Shift Keying): Information is encoded in the time of release of information particles [33, 34], as depicted in Fig. 2.5. For example, the transmitter can send a molecule at $t = 0$ s to represent the bit "1" and send a molecule at $t = \tau, \tau > 0$ s to represent the bit "0". If the receiver detects a molecule arriving at a time before $t = \tau$ during the

current transmission interval, it can decide that the bit "1" was sent by the transmitter. Otherwise, the receiver can decide that the bit "0" was sent by the transmitter.

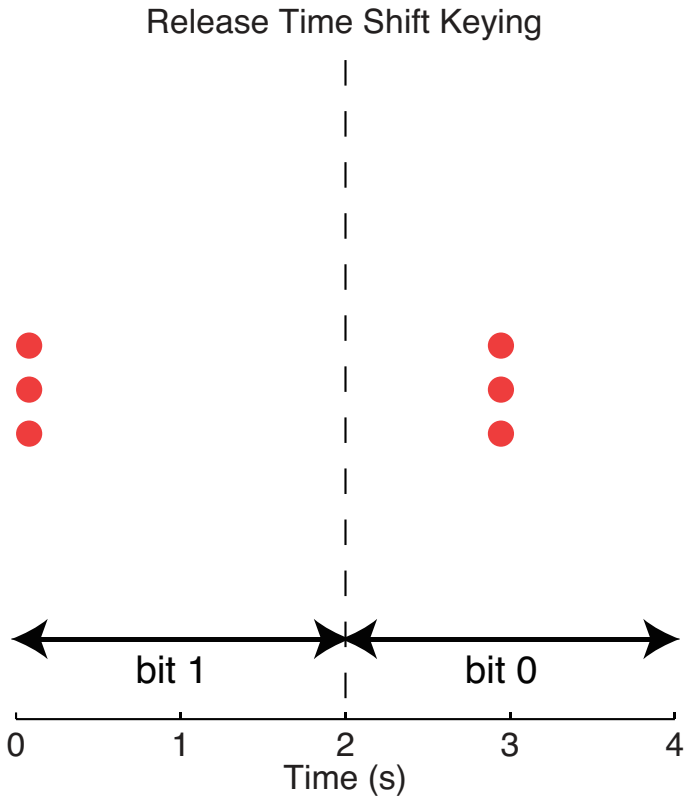

Figure 2.5: An example of modulating on the timing of molecules in MC [2]. In this example, during time $t = [0, 2)$ s, the transmitter releases molecule(s) for the first bit of information and during time $t = [2, 4)$ s, the transmitter releases molecule(s) for the second bit of information. In this example, the transmitter releases three molecules (represented by red dots) at the beginning of the bit interval to express the bit "1" for the first bit and releases three molecules 1 s later than the beginning of the bit interval to express the bit "0" for the second bit.

2.3 Propagation Schemes

The propagation schemes in the literature are usually categorized as passive propagation and active propagation. Passive propagation is realized by the stochastic diffusion of molecules. This propagation scheme is simple for mathematical calculation. Hence, passive propagation has been adopted widely in the theoretical system models in MC studies. Active propagation, on the other hand, uses mobile bio-nanomachines to carry molecules in a certain direction. For example, protein motors can carry information particles in networks that are built with protein filament [37].

Pure diffusion is the simplest example of passive propagation schemes, where molecules diffuse according to Brownian motion. This means that the propagation uses kinetic energy only and no external source of energy is used. In pure diffusion, molecules spread throughout the environment as a result of Brownian motion. Some of the information-carrying molecules arrive at the receiver during the time interval of transmitting a single bit and the characteristics of the arrived molecules can be interpreted into the received signal. Pure diffusion is the most fundamental and a widely used propagation scheme in MC systems, due to its simplicity and energy-efficient nature. An example of pure diffusion in biology is the nerve cells sending signals to muscle tissue [38].

Considering communication over a long transmitter-to-receiver distance, the propagation speed of pure diffusion can be extremely slow. Therefore, there are various ways in assisting the diffusion of molecules, which include:

1. **Flow assisted propagation**: Propagation can be supported by the communication medium. A flow introduced to the medium can improve the propagation speed. An effective way in performing flow assisted propagation is to introduce a flow that is in the direction from the transmitter to the target receiver. An example in nature is the blood vessels carrying molecules to distant target cells inside the human body.

2. **Motor protein assisted propagation**: Motor proteins can help moving information particles. Specifically, propagation with microtubules and kinesin motor proteins is another solution to assist molecule diffusion [8, 23]. Microtubules are tube-shaped structures that are usually involved in intracellular transport in nature and kinesin motors can carry molecules following the tracks of microtubules from transmitters to receivers.

3. **Bacteria assisted propagation**: Bacteria can help propagate information-carrying molecules from transmitters to receivers [39, 40]. Information-carrying molecules are placed inside bacteria for transportation. The loaded bacteria are released into the environment by the transmitter and propagate until they reach the target receiver.

2.4 Absorbing Receiver Models

One of the major challenges in designing and analyzing diffusion-based MC systems is receiver modeling. The majority of existing MC studies have considered two types of receivers: passive receivers and active receivers [2, 41]. Passive receivers do not impose any impact on molecule propagation, while active receivers have some mechanism for molecules to adsorb to or react with the receiver. Compared to passive receivers, active receivers are more practical and can better represent typical biological receivers.

The attempts to find analytical solutions for diffusion-based MC systems with absorbing receivers started from one-dimensional (1D) systems [20, 42]. [20] considered a diffusion-based MC system with drift and a perfectly absorbing receiver and presented the PDF of the first passage time of molecules. [42] considered a diffusion-based MC system with molecule degradation and a perfectly absorbing receiver and presented the PDF of the first passage time of molecules.

For a spherical absorbing receiver, the first work on the channel response of an MC system with an irreversible perfectly absorbing receiver is [43]. In this work, the authors considered a spherical receiver with a perfectly absorbing boundary. A point transmitter is located at the origin of a Cartesian coordinate system and the spherical absorbing receiver is centered on the x-axis. Molecules are released simultaneously from the point transmitter into the environment at the start of the simulation process and propagate freely in the environment since being released. The authors also presented analysis on the absorption rate and the fraction of absorbed molecules for the considered system model. They further derived the signal delay and path loss functions. Following [43], in [9] the authors considered the same system model as in [43] and explored the first time hitting probability and concentration distribution of particles for the model. They further presented a simulation framework for the proposed model and provided additional information on the channel model verification, modulation, as well as interference mitigation.

It is noted that reversible spherical absorbing receivers are more complicated than irreversible ones. In [44], the authors considered an absorption and desorption receiver, which means that an absorbed molecule can be released back to the environment at some time after the absorption, and the desorption is determined by a desorption rate. The desorption of absorbed molecules is not a rare case in nature. Particularly, it is widely observed in the processes of colloids, proteins, and polymers. Thus, in [44] authors derived the net number of absorbed molecules for an

MC system with a reversible absorbing receiver, presented a simulation algorithm, and analyzed the error performance of the considered system model. It was found that the error probability decreases when the absorption rate grows or when the desorption rate decreases. This is because that an absorbing receiver can direct the molecules toward the receiver and as a result, enhance the transmission performance. The authors also discovered that the considered system requires a lower detection threshold than perfectly or partially absorbing receivers.

As an advancement over the aforementioned studies which have focused on point-to-point communications, [5] addressed a broadcast model. In [5], the authors investigated the MC system with multiple non-overlapping absorbing receivers by evaluating the asymptotic fractions of the molecules absorbed by receivers as the transmission time goes large. Perfectly absorbing receivers are deployed symmetrically around the point transmitter which is located at the origin. Once a molecule walks into one of the receivers, it is considered as absorbed. The absorption probability of molecules was examined for both the single-receiver scenario and the multi-receiver scenario. However, for the multi-receiver scenario, no analytical expression exists for the absorption probability. Hence, the simulation results were presented together with the single-receiver analytical results. The authors also improved the accuracy of the simulation algorithm for absorbing receivers by introducing an intra-step absorption probability for planar boundaries, which was first proposed in [4], to approximate the intra-step absorption probability for spherical boundaries.

2.5 Channel Characterization

Focusing on diffusion-based MC systems with point sources and spherical receivers but without drift, in this section we review the existing analysis of the channel impulse response of a system with a single passive receiver and that of a system with a single absorbing receiver.

The macroscopic theory of diffusion is developed based on two assumptions. The first assumption is on the relation between flux and concentration, i.e., substances move from the high concentration region to the low concentration region, down the concentration gradient. The second assumption is on mass conservation, i.e., a steeper gradient results in more movement of substances [45]. Let us consider an ideal three-dimensional (3D) system where the diffusion coefficient is independent of concentration and there is no flow in the environment. For a diffusion process where molecules are released from the origin of a Cartesian coordinate system, we

combine the two aforementioned assumptions and write the derivative of the flux as

$$\frac{\partial C(r,t)}{\partial t} = D\nabla^2 C(r,t), \tag{2.1}$$

where ∇ is the Laplacian operator, $C(r,t)$ represents the concentration of molecules at time t and at location r.

For a pure diffusion 3D MC system that has a point source transmitter, without the presence of a receiver, the solution to the concentration at a distance r from the point source in an infinite environment is solved as

$$C(r,t) = \frac{N}{8(\pi D t)^{\frac{3}{2}}} \exp\left(-\frac{r^2}{4Dt}\right). \tag{2.2}$$

If there is a passive receiver with a volume of V in the system that does not impose any impact on molecules, the expected observed number of molecules at the receiver volume is given by

$$\overline{N(t)} = \int_V C(r,t)\mathrm{d}V. \tag{2.3}$$

For a pure diffusion 3D MC system that has a point source transmitter, a number of N molecules released by the transmitter at the beginning of the transmission, $t = 0$, and an absorbing receiver that removes some of the molecules from the environment when they reach the receiver, we can solve the concentration of information molecules in the system at time t and at a distance r from the transmitter after defining the following conditions. First, the initial condition is given by

$$C(r,t) = \frac{N}{4\pi {r_0}^2}\delta(r - r_0), \tag{2.4}$$

where r_0 is the initial distance from the transmitter to the center of the absorbing receiver. Also, the boundary conditions that consider the impact of the absorbing receiver are expressed as

$$\lim_{r\to\infty} C(r,t) = 0, \tag{2.5}$$

which means that molecules vanish at a distance sufficiently far from the receiver and the transmitter, and

$$D\frac{\partial C(r,t)}{\partial r} = vC(r,t) \text{ at } d_{\mathrm{RX}} = r_{\mathrm{r}}, \tag{2.6}$$

where d_{RX} is the distance from a location to the receiver, r_{r} is the radius of the spherical receiver which is assumed to be smaller than r_0, and v is the rate constant representing the proportion of concentration of particles that reacts with the receiver

in a unit of time. It is indicated by (2.6) that at the receiver surface, the number of molecules that react with the receiver equals the number of molecules that disappear from the environment. For a perfectly absorbing receiver that absorbs every collided particle, the time-varying concentration of molecules diffusing in the environment at time t and at a distance r from the transmitter is expressed as

$$C(r,t) = \frac{N}{4\pi r r_0 \sqrt{4\pi D t}} \left(\exp\left(-\frac{(r-r_0)^2}{4Dt} \right) - \exp\left(-\frac{(r+r_0-2r_\mathrm{r})^2}{4Dt} \right) \right). \quad (2.7)$$

The number of molecules absorbed by the receiver surface until given time t is obtained by integrating (2.7) over receiver surface area and time period, given by

$$N(t) = \frac{N r_\mathrm{r}}{r_0} \mathrm{erfc}\left(\frac{r_0 - r_\mathrm{r}}{\sqrt{4Dt}} \right). \quad (2.8)$$

2.6 Experimental Systems and Prototype

There are a limited number of existing studies on the development of experimental MC systems, due to the high expenses and the strong requirements for interdisciplinary background knowledge. Despite these difficulties, [46] and [47] are two pioneer studies that considered experimental MC models. In [46], messages were sent by transmitter artificial cells and detected and decoded by receiver artificial cells. In [47], messages to be conveyed are encoded into DNA.

While the aforementioned experimental systems focus on microscale explorations, some recent efforts have been devoted to the development of macroscale prototype, e.g., [48]. Specifically, [48] presented the first tabletop MC prototype and was named Kinboshi, which has the capability to transmit short text messages through the propagation of alcohol molecules over air. Importantly, it requires a low cost to operate. In this prototype, text messages are encoded into binary sequences, and alcohol molecules are released to represent bits of information in the sequence using ON-OFF keying modulation. The propagation of alcohol molecules in Kinboshi is assisted by an air flow generated by a fan. Finally, the performance of this prototype was demonstrated and discussed.

2.7 Software-Based Simulation Methods

The majority of the previous studies on MC models benefit from simulations. In this section, we review some existing simulation frameworks for MC systems and then particularly look into particle-based microscopic simulation algorithms for diffusion-based MC systems with absorbing receiver(s).

2.7.1 Existing simulation frameworks

In MC, simulations often serve as an effective method of investigating the performance of a communication system. There exist, from the broader topic of molecular science, some general solvers that model the behavior of molecules over various physical scales and environmental settings, such as the commercial continuum solvers COMSOL [49] and ANSYS [50] that perform deterministic dynamic simulations, the Smoluchowski Dynamics simulator (Smoldyn) that considers a uniform time step and tracks molecules over discrete time steps [51], and the event-based Green's function reaction dynamics (GFRD) technique that considers a maximum simulation time step and tracks changes in molecules' discrete states [52].

However, general molecular simulation solvers are not easy to be applied into the research of MC for a few reasons [6]. First, the releasing patterns of transmitters in general solvers are rarely designed to accommodate the common modulation techniques in MC. Second, the focus of simulation in MC is on the behavior of molecules at the receivers, while in other fields, the system behavior needs to be closely monitored everywhere. Third, for MC, the Monte Carlo method is widely applied to generate channel statistics and such application cannot be easily achieved using general solvers.

Due to the aforementioned reasons, a number of simulation frameworks have been developed to particularly examine the behavior of information particles in MC environments. They are summarized as follows:

- BNSim (Bacterial Network Simulator) is a mesoscopic simulator that implements diffusion-based MC in a 3D space using a reaction-diffusion algorithm for bacteria-based communication systems [53]. Bacteria that undergo chemotaxis, quorum sensing, or light-based intercellular signaling are considered.
- BiNS2 (Biological Nanoscale Simulator) is a microscopic simulator that considers diffusion with reaction and uses a space partition algorithm [54]. Trans-

mitter and receiver devices are mobile in BiNS2 and information molecules are detected by receptors. Users can customize and modularize the simulation environment.

- N3Sim is a Java based microscopic simulator [55]. It is a simulation tool for diffusion-based MC. It evaluates the performance of MC systems in both two-dimensional (2D) and 3D environments for specific scenarios. It uses Brownian motion and considers particle inertia and collisions among molecules. Receivers can be either passive or active in N3Sim.

- MUCIN (MolecUlar CommunicatIoN) is a microscopic simulator for unbounded 3D environments. It is a simulation tool developed based on MATLAB [9]. A transmitter releases molecules according to various modulation schemes. The spherical receiver can be a passive receiver, a partially absorbing receiver, or a perfectly absorbing receiver. Together with the framework, the authors also presented a case study to analyze intersymbol interference mitigation and carry out a performance evaluation on the MC system.

- NanoNS3 is a continuum simulator for bacteria-based communication systems [56]. It is developed based on the NS-3 discrete simulator. The simulator uses the models that accurately describe receiver response, microfluidic channel loss, and modulation schemes.

- AcCoRD (Actor-based Communication via Reaction-Diffusion) is a sandbox simulator that considers diffusion with reaction [6]. It is a simulation tool developed based on C and can output results in MATLAB. It is able to use hybrid of microscopic and mesoscopic simulation approaches to simulate time-varying molecule behaviors.

The development of the aforementioned simulation frameworks can be categorized as three major simulation approaches, namely, the microscopic approach, the mesoscopic approach and the hybrid approach [57]. Considering a sub-region of the simulation environment, the microscopic approach treats the molecules within the region individually, while the mesoscopic approach treats them in aggregate as uniformly distributed throughout the region. A detailed comparison between the microscopic and mesoscopic approaches and further information on how they have been implemented in MC frameworks were shown in [2, 6]. In this project, we choose to study the microscopic simulation approach since this approach is commonly used in simulation algorithms for diffusion with reaction systems. A widely recognized example of the microscopic approach in MC is the particle-based simulation that uses Brownian motion to characterize particle propagation.

2.7.2 Microscopic simulation of Brownian motion

There are various techniques that simulate the diffusion of particles. A commonly used and more direct technique is considered in this thesis, which is particle-based tracking. The key idea is to discretize space and time, and describe the trajectory of a particle by using the probability density of finding the particle at a particular position at a given time.

For a 3D environment, the movement of a particle in a single time step can be modeled as three independent random variables on three directions, all of which follow a Gaussian distribution with zero mean and σ^2 variance. Mathematically, the x-, y-, and z- coordinates of a molecule that propagates according to Brownian motion at the end of the ith time step, $i > 0$ and i is an integer, can be approximated as

$$\begin{aligned} x_i &= x_{i-1} + \mathcal{N}(0, \sigma^2), \\ y_i &= y_{i-1} + \mathcal{N}(0, \sigma^2), \end{aligned} \tag{2.9}$$

and

$$z_i = z_{i-1} + \mathcal{N}(0, \sigma^2),$$

respectively. This indicates that the coordinates are approximated as discrete functions of time for the sake of simulation, although in reality the movements of molecules undergoing Brownian motion are continuous over both time and space.

2.7.3 Intra-step probability for simulating absorbing receivers

It has been noted in the existing studies that the simulation framework for an absorbing receiver in diffusion-based MC systems does not match the analytical expression very well when the simulation time step or the diffusion coefficient value is large. In an example of the conventional simulation algorithms for absorbing receivers, referred to as the simplistic Monte Carlo (SMC) algorithm [5], only the molecules that have been observed inside the spherical receiver at the end of simulation time steps had the chances to become absorbed. This means that when the simulation time step increases, the simulated fraction of absorbed molecules becomes much smaller than the actual value. For a planar absorbing boundary, the probability of molecule absorptions happening during simulation time steps was solved in [4]. Two of the existing simulation algorithms that attempted to tackle this issue for spherical receivers were presented and discussed in [6] and [5].

In [6], a molecule is absorbed if the line segment from its initial position to its final position during the current simulation time step crosses the receiver's boundary. However, we note that the line segment crossing the receiver's surface is neither sufficient nor necessary to correctly detect intra-step absorption. The accuracy of the algorithm in [6] is better than but still comparable to the SMC algorithm.

In [5], the authors contributed to the simulation of absorbing receivers in diffusion-based MC systems by introducing an approximated probability of a molecule being absorbed during simulation time steps. This simulation algorithm was referred to as the refined Monte Carlo (RMC) algorithm. Inspired by the calculation of the probability of absorptions happening during simulation time steps for a planar absorbing boundary, they performed a similar calculation to approximate the absorptions for a spherical absorbing surface. As it turned out, the calculation is still accurate for a spherical absorbing boundary when the simulation time step is relatively small. Based on this, they presented simulation results for spherical absorbing receivers and showed that the approximation works very well for a time step length up to 100 ms. However, as we have tested, when the step length increases to a value larger than 100 ms or when the diffusion coefficient further increases, the accuracy of this approximation starts to become worse. This motivates us to propose a new simulation algorithm which aims to increase the accuracy of simulation when a much larger time step length is used.

Chapter 3

System Model

As demonstrated in Chapter 2, the conventional simulation algorithms for absorbing receivers in diffusion-based MC systems often underestimate the probability of molecules being absorbed when the simulation time step length is relatively large. Thus, there are some recent advancements that improve the accuracy of existing algorithms on simulating absorbing receiver(s) [5, 6].

In this chapter, we first consider a diffusion-based MC system with a single absorbing receiver and review the analytical fraction of molecules absorbed in this scenario. The analytical fraction will be used to evaluate the performance of various simulation algorithms later. Then, we consider a diffusion-based MC system with multiple absorbing receivers and we review the long-time reaction probability of a molecule with one of the absorbing receivers especially for a symmetric two-receiver system. Finally, we describe the intra-step absorption probability that leads to the inaccuracy of existing algorithms and explain some of the expressions utilized in recent approaches that achieved advancements on producing more accurate simulation results.

3.1 A Single Absorbing Receiver in Diffusion-Based MC

3.1.1 System description

We consider a diffusion-based MC system within an infinite 3D environment, represented by a Cartesian coordinate space, as depicted in Fig. 3.1. The propagation in the environment only depends on Brownian motion. In this system, a point transmitter (TX) is located at the origin of the Cartesian coordinate and a spherical absorbing receiver (RX) is centered at location $(r_0, 0, 0)$. We denote r_r as the RX's

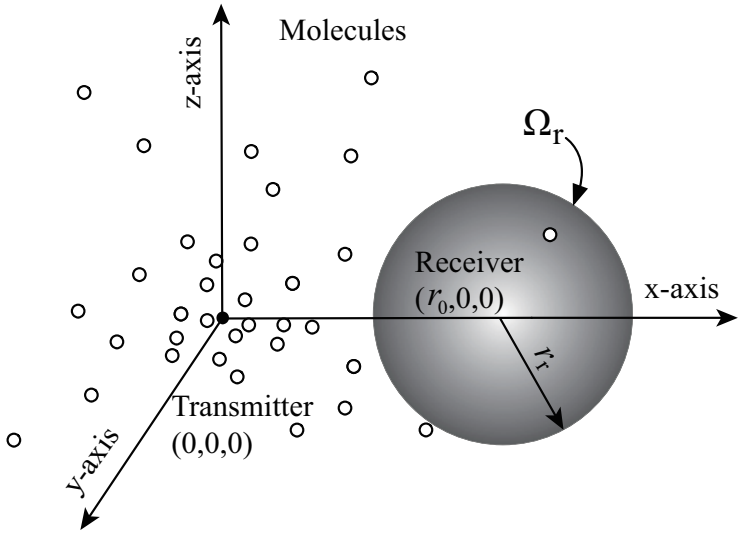

Figure 3.1: Illustration of our system model with a single absorbing RX. The TX is a point transmitter located at $(0, 0, 0)$, the RX is a spherical perfectly absorbing RX located at $(r_0, 0, 0)$ with r_r being the radius and Ω_r being the RX's perfectly absorbing boundary. Molecules propagate in the environment according to Brownian motion until hitting the absorbing boundary of the RX.

radius, which is assumed to be smaller than r_0, and Ω_r as the RX's boundary.

At the beginning of a transmission process, the TX instantaneously releases N molecules into the environment. Once released, molecules are detectable if they appear inside or on the surface of the RX. We assume that the molecules are small enough to be considered as points and each molecule diffuses independently. We also assume that Ω_r is perfectly absorbing, which means every molecule that crosses Ω_r will be absorbed and removed from the environment. We further assume that the RX is able to count the number of absorbed molecules until a given time.

3.1.2 Channel impulse response

We denote $N_\mathrm{RX}\left(\Omega_\mathrm{r}, t|r_0\right)$ as the mean number of molecules that are released from the TX at time $t_0 = 0\,\mathrm{s}$ and absorbed by the RX by time t. As per [58, Eq. (3.116)], we express $N_\mathrm{RX}(\Omega_\mathrm{r}, t|r_0)$ as

$$N_\mathrm{RX}\left(\Omega_\mathrm{r}, t|r_0\right) = \frac{N r_\mathrm{r}}{r_0}\mathrm{erfc}\left(\frac{r_0 - r_\mathrm{r}}{\sqrt{4Dt}}\right), \tag{3.1}$$

where D is the diffusion coefficient and $\mathrm{erfc}\left(\cdot\right)$ is the complementary error function. (3.1) is of significant importance in this thesis, since that the performance of simulation algorithms will be examined by comparing their produced results to the results calculated using (3.1). Details on the performance evaluation of simulation

algorithms will be given later in Chapter 5.

3.2 Multiple Absorbing Receivers in Diffusion-Based MC

3.2.1 System description

We now consider a system containing multiple absorbing spherical RXs. In an infinite 3D MC system represented by a Cartesian coordinate space, a point TX stays at the origin of the space and l RXs are scattered around the TX. The absorbing RXs have radii of $r_{\mathrm{r}i}$, $i \in \{1, 2, ...l\}$, and their centers are at distances of $d_{\mathrm{TX-RX},i}$ away from the TX. We assume that $r_{\mathrm{r}i} < d_{\mathrm{TX-RX},i}$ for all values of i. At the beginning of a transmission, the TX releases N molecules into the system and molecules propagate according to Brownian motion until hitting the boundary of one of the RXs.

Based on this multiple absorbing RXs model, we will present in Chapter 5 the simulation results of the averaged fractions of molecules absorbed by the RXs using different algorithms and compare them. Also, for this general model, we note that there is no analytical time-varying expression for the fraction of molecules absorbed by each RX in literature. Therefore, we specifically look into the case of two identical absorbing RXs locating on opposite sides of and equidistant from the TX, since there exists theoretical analysis for the probability of a molecule eventually being absorbed by one of two absorbing RXs for this scenario. This probability analysis will provide further insights when comparing the performance of algorithms. We will also present the simulation results for the case of four identical absorbing RXs in Chapter 5. These two particular cases of multiple absorbing RXs model will provide fundamental results to deal with more general MC systems which may be of greater interests.

3.2.2 Long-time reaction probability

For the case of two identical absorbing RXs locating on opposite sides of and equidistant from the TX, we denote $\mathrm{Pr}_{\mathrm{RX},i}(t \to \infty)$, $i \in \{1, 2\}$, as the probability of a molecule eventually being absorbed by one of two absorbing RXs, where t is the transmission time.

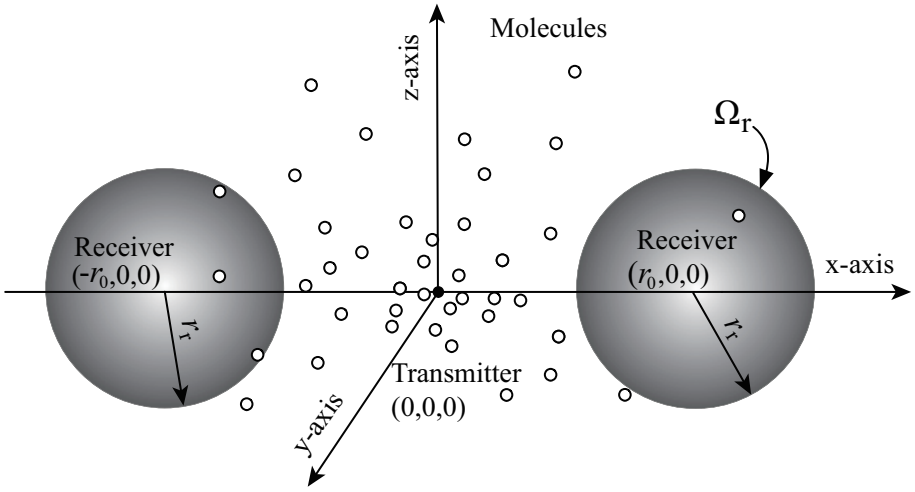

Figure 3.2: Illustration of our two absorbing RXs system model. The TX is a point transmitter located at $(0, 0, 0)$, two perfectly absorbing RXs are located on opposite sides of and equidistant from the TX. The two absorbing RXs have the same radius r_r and their centers are separated by a distance of $2r_0$, $r_0 > r_\mathrm{r}$. Molecules propagate in the environment according to Brownian motion.

Taking into account the symmetry of the system with respect to the xy plane, we know that the two probabilities are identical. Hence, we also use $\mathrm{Pr}_{\mathrm{RX},1\&2}(t \to \infty)$ to represent the identical probabilities. To solve the probabilities, we first recall that $\mathrm{Pr}_{\mathrm{RX},1\&2}(t \to \infty)$, satisfies the steady-state backward diffusion equation, which is given by

$$\nabla^2 \mathrm{Pr}_{\mathrm{RX},1\&2}(t \to \infty) = 0. \tag{3.2}$$

The bispherical coordinate system is the natural environment for solving this problem [59], of which the coordinates (μ, η, ϕ) are defined by

$$\begin{aligned} x &= \frac{I \sin\eta \cos\phi}{\cosh\mu - \cos\eta}, \\ y &= \frac{I \sin\eta \sin\phi}{\cosh\mu - \cos\eta}, \\ z &= \frac{I \sinh\mu}{\cosh\mu - \cos\eta}, \end{aligned} \tag{3.3}$$

where $\mu \in (-\infty, \infty)$, $\eta \in [0, \pi]$, $\phi \in [0, 2\pi]$, and I is the interfocal distance. The surfaces of μ are given by

$$x^2 + y^2 + (z - I\coth\mu)^2 = \frac{I^2}{\sinh\mu^2}, \tag{3.4}$$

and the surfaces of η are given by

$$x^2 + y^2 + z^2 - 2I\sqrt{x^2 + y^2}\cot\eta = I^2. \tag{3.5}$$

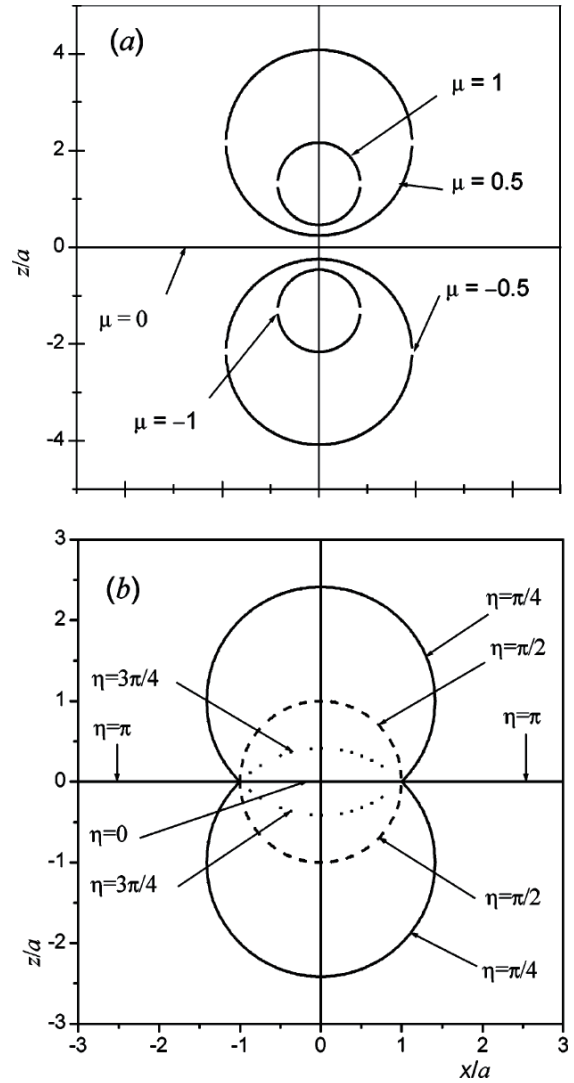

Figure 3.3: The isosurfaces of the bispherical coordinates. (a) Surfaces of constant μ, (b) Surfaces of constant η. The surfaces are obtained by rotating the section about the z-axis of the bispherical coordinates [3].

Examples of the surfaces of μ and η at various constant values are shown in Fig. 3.3. The ϕ coordinate represents the longitude angle and the surfaces of ϕ are given by half-planes. Cartesian coordinates (x, y, z) can be transformed to bispherical coordinates with

$$\mu = \tanh^{-1}\left(\frac{2Iz}{x^2 + y^2 + z^2 + I^2}\right), \tag{3.6}$$

$$\eta = \cos^{-1}\left(\cosh\mu - \frac{I}{z}\sinh\mu\right), \tag{3.7}$$

and

$$\phi = \tan^{-1}(y/x). \tag{3.8}$$

For a system with two spherical RXs that have the same radius $r_{\mathrm{r}1} = r_{\mathrm{r}2} = r_{\mathrm{r}0}$,

the centers of the two RXs separated by a distance of $d_{\mathrm{TX-RX},1} + d_{\mathrm{TX-RX},2} = 2r_0$, the absorbing surfaces of RXs in the bispherical coordinate system are expressed as $\mu_1 = \cosh^{-1}(r_0/r_{\mathrm{r}0})$, $\mu_2 = -\cosh^{-1}(r_0/r_{\mathrm{r}0})$ and we find that $I = r_{\mathrm{r}0}\sinh|\mu|$. Using the bispherical coordinate system, the steady-state backward diffusion equation becomes [60]

$$\frac{\partial^2 U}{\partial \mu^2} + \frac{1}{\sin\eta}\frac{\partial}{\partial \eta}\left(\sin\eta\frac{\partial U}{\partial \eta}\right) + \frac{1}{\sin^2\eta}\frac{\partial^2 U}{\partial \phi^2} - \frac{1}{4}U = 0, \tag{3.9}$$

where $U = (\cosh\mu - \cos\eta)^{\frac{1}{2}}\mathrm{Pr}_{\mathrm{RX},1\&2}(t \to \infty)$. A general solution to this equation is given in [60, 61]

$$\begin{aligned}\mathrm{Pr}_{\mathrm{RX},1\&2}(t \to \infty) =& \sqrt{(\cosh\mu - \cos\eta)} \\ &\times \sum_{n=0}^{\infty}(A_n \mathrm{e}^{(n+1/2)\mu} + B_n \mathrm{e}^{-(n+1/2)\mu})P_n(\cos\eta),\end{aligned} \tag{3.10}$$

where A_n and B_n are the same when the spherical sinks are identical and P_n is the nth-degree Legendre polynomial.

To solve the probability of a released molecule being absorbed by RX_1 in the system with two spherical RXs, the appropriate boundary conditions for solving the arbitrary constants in (3.10) are found as

$$\mathrm{Pr}_{\mathrm{RX},1}(t \to \infty) = 1, \text{at } d_{\mathrm{TX-RX},1} = r_{\mathrm{r}0}, \tag{3.11}$$

$$\mathrm{Pr}_{\mathrm{RX},1}(t \to \infty) = 0, \text{at } d_{\mathrm{TX-RX},2} = r_{\mathrm{r}0}, \tag{3.12}$$

$$\mathrm{Pr}_{\mathrm{RX},1}(t \to \infty) = 0, \text{when } d_{\mathrm{TX-RX},1}\&d_{\mathrm{TX-RX},2} \to \infty, \tag{3.13}$$

where $d_{\mathrm{TX-RX},1}$ and $d_{\mathrm{TX-RX},2}$ represent the $\mathrm{TX} - \mathrm{RX}_1$ and $\mathrm{TX} - \mathrm{RX}_2$ distances, respectively. With boundary conditions (3.11), (3.12), and (3.13), the exact solution to (3.10) for the two identical RXs scenario is obtained as

$$\begin{aligned}\mathrm{Pr}_{\mathrm{RX},1}(t \to \infty) =& \sqrt{2\,(\cosh\mu - \cos\eta)} \\ &\times \sum_{n=0}^{\infty}\mathrm{e}^{-\left(n+\frac{1}{2}\right)\mu_1}\frac{\sinh\left(n+\frac{1}{2}\right)(\mu-\mu_2)}{\sinh\left(n+\frac{1}{2}\right)(\mu_1-\mu_2)}P_n\left(\cos(\eta)\right).\end{aligned} \tag{3.14}$$

Similarly, the probability of a released molecule being absorbed by RX_2 in the system can be obtained.

Proof. With general solution (3.10) and boundary conditions (3.11), (3.12), and (3.13), we obtain (3.14) as follows [3, 61]:

Substituting $\mu = \mu_1$ into (3.10) and using (3.11), we obtain

$$\frac{1}{\sqrt{(\cosh\mu_1 - \cos\eta)}} = \sum_{n=0}^{\infty}\left(A_n \mathrm{e}^{(n+\frac{1}{2})\mu_1} + B_n \mathrm{e}^{-(n+\frac{1}{2})\mu_1}\right)P_n(\cos\eta). \tag{3.15}$$

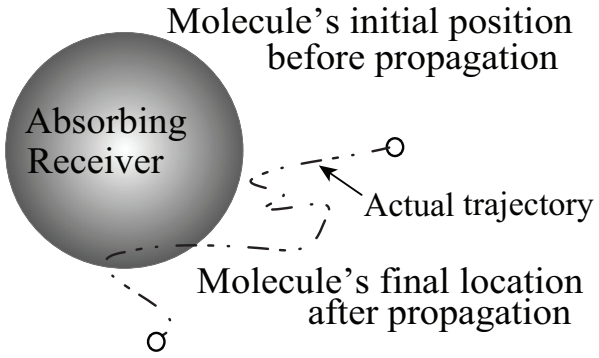

Figure 3.4: Illustration of the intra-step molecule movement for a spherical boundary. There is a possibility that a molecule crosses an absorbing boundary within one time step, even if its initial and final positions during that time step are both outside the absorbing RX.

Then, by using Legendre series expansion [62], (3.15) becomes

$$\sqrt{2}\sum_{n=0}^{\infty} \mathrm{e}^{-(n+\frac{1}{2})|\mu_1|} P_n(\cos\eta) = \sum_{n=0}^{\infty} \left(A_n \mathrm{e}^{(n+\frac{1}{2})\mu_1} + B_n \mathrm{e}^{-(n+\frac{1}{2})\mu_1} \right) P_n(\cos\eta). \quad (3.16)$$

After that, substituting $\mu = \mu_2$ into (3.10) and using (3.12), we obtain

$$0 = \sum_{n=0}^{\infty} \left(A_n \mathrm{e}^{(n+\frac{1}{2})\mu_2} + B_n \mathrm{e}^{-(n+\frac{1}{2})\mu_2} \right) P_n(\cos\eta). \quad (3.17)$$

Finally, solving (3.16) and (3.17) gives (3.14). □

3.3 Intra-Step Probability Analysis

As mentioned in Chapter 2, when determining the absorption of molecules in particle-based simulations, some existing algorithms simply compare the observed coordinates of molecules with the coordinates of the RX [9, 44, 55] at the end of every simulation time step, as will be shown in details in Chapter 4.

However, the actual trajectory of a molecule may cross the RX boundary during one simulation time step, even if its initial position at the beginning of the time step and its final position at the end of the same time step are both outside the absorbing RX. As a consequence of ignoring this crossing, the molecules that hit the RX in during simulation time steps cannot be considered as "absorbed" by using these

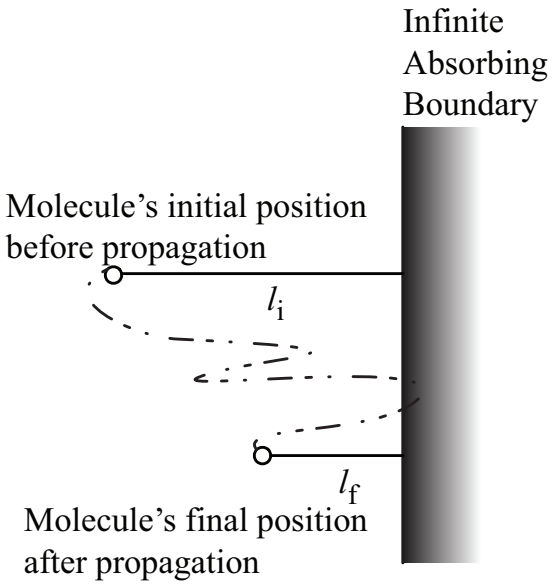

Figure 3.5: Illustration of the intra-step molecule movement for a system with an infinite flat planar boundary. There is a possibility that a molecule crosses an absorbing boundary during one simulation time step, even if its initial and final positions for that time step are both outside the absorbing RX [4].

simulation algorithms. This ignored absorption is as depicted in Figs. 3.4 and 3.5, and we refer to it as the *intra-step molecule absorption*.

In this thesis, we refer to the probability that a molecule is absorbed by an RX during a simulation time step as the *intra-step absorption probability*. Recently, [5] and [6] investigated the intra-step absorption probability. Specifically, [5] approximated the intra-step absorption probability for spherical RX boundaries using the equation for flat planar RX boundaries given by [4, Eq. (10)]. Alternatively, [6] declared a molecule as "absorbed" if its straight-line trajectory within a simulation time step crossed an absorbing surface.

We now look into the details of the approximation of intra-step absorption probability used in [5]. As depicted in Fig. 3.5, the intra-step absorption probability for a molecule in a system that has an infinite flat planar absorbing boundary is calculated as [4]

$$\mathrm{Pr}_{\mathrm{intra},\Omega_{\mathrm{p}}} = \exp\left(-\frac{l_{\mathrm{i}} l_{\mathrm{f}}}{D\Delta t}\right), \tag{3.18}$$

where l_{i} and l_{f} are labeled as in Fig. 3.5, Ω_{p} denotes the infinite flat planar absorbing boundary and Δt is the simulation time step length.

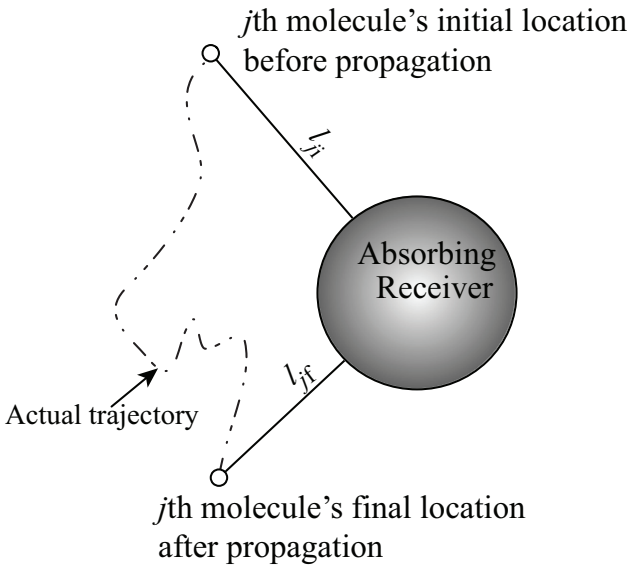

Figure 3.6: Illustration of the distances used in the intra-step absorption probability calculation in the RMC algorithm [5].

Proof. Given that 1) the initial and final distances from the molecule to the flat planar boundary are l_i and l_f for the current simulation time step, 2) Prob is a probability, prob is the corresponding probability density of Prob, and 3) the Gaussian profile for the movement of molecule on each coordinate of three is

$$G(l) = \frac{1}{\sqrt{4\pi D\Delta t}} \exp\left(-\frac{l^2}{4D\Delta t}\right), \tag{3.19}$$

the intra-step absorption probability for an infinite flat planar boundary is then given by [4]:

$$\begin{aligned} \mathrm{Pr}_{\mathrm{intra},\Omega_\mathrm{p}} &= 1 - \mathrm{Prob}(\text{no intra} \mid l_\mathrm{f}) \\ &= \frac{\mathrm{prob}(l_\mathrm{f}) - \mathrm{prob}(\text{no intra}, l_\mathrm{f})}{\mathrm{prob}(l_\mathrm{f})} \\ &= \frac{G(l_\mathrm{f} - l_\mathrm{i}) - (G(l_\mathrm{f} - l_\mathrm{i}) - G(l_\mathrm{f} + l_\mathrm{i}))}{G(l_\mathrm{f} - l_\mathrm{i})} \\ &= \exp\left(-\frac{l_\mathrm{i} l_\mathrm{f}}{D\Delta t}\right), \end{aligned} \tag{3.20}$$

where "no intra" means the molecule has not crossed the boundary at all for the current time step. □

Then, applying the same approximation method for a spherical RX, we denote d_j as the distance between the jth molecule and the TX, $j \in \{1, 2, ...N\}$. The shortest distance between the jth molecule and the RX boundary at the beginning of the current simulation time step is written as $l_{j\mathrm{i}}$, and the shortest distance between the jth molecule and the RX boundary at the end of the current simulation time

step is written as $l_{j\mathrm{f}}$, as shown in Fig. 3.6. We then have $\mathrm{Pr}_{\mathrm{RMC}}$ that describe the approximated intra-step absorption probability used by the RMC algorithm to determine the absorption of the jth molecule. It is given by [5]

$$\mathrm{Pr}_{\mathrm{RMC}} = \mathrm{Pr}_{\mathrm{intra},\Omega_{\mathrm{r}}} = \exp\left(-\frac{l_{j\mathrm{i}} l_{j\mathrm{f}}}{D\Delta t}\right). \tag{3.21}$$

Chapter 4

Simulation Algorithms

In this chapter, we explore algorithms on simulating the number of molecules absorbed by perfectly absorbing RX(s) in diffusion-based MC. We first describe some of the existing simulation algorithms for a single absorbing RX. Then we propose polynomial functions to predict the accuracy of the RMC algorithm given the system parameters. After that, we present our proposed APMC algorithm and determine the likelihood threshold to be applied to both the APMC and RMC algorithms in order to reduce computational complexity. Finally, we modify the APMC and RMC algorithms to investigate the performance of algorithms in the simulation of MC systems with multiple absorbing RXs.

4.1 Existing Simulation Algorithms

4.1.1 Absorption criterion

By observing the existing simulation algorithms for microscopic molecule absorption in diffusion-based MC (such as those in [5, 6, 9]), we identify that they follow a common structure. For each simulation time step, all algorithms first scan for free molecules, propagate them according to Brownian motion, and then decide the molecules to be absorbed in the current time step. The main difference among algorithms is that each algorithm has its own criterion for determining whether or not a molecule is absorbed by the RX. We describe the criterion of each of them as follows:

- As per the determination criterion in [9], only the molecules observed inside the RX at the end of every simulation time step are absorbed. This criterion is referred to by [5] as the simplistic Monte Carlo (SMC) algorithm. However, we note from simulation results in [5] that the SMC algorithm is inaccur-

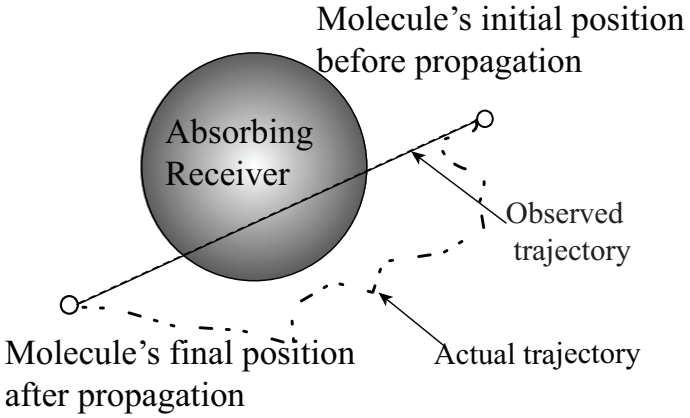

Figure 4.1: An example which shows the inaccuracy of the determination criterion in [6]. In this example, the line segment from the molecule's initial position to its final position in the current simulation time step crosses the RX's surface, indicating that this molecule is absorbed by the RX as per the determination criterion in [6]. However, the molecule's actual trajectory indicates that this molecule is not absorbed.

ate, unless the simulation time step is *very* small. This is because the SMC algorithm ignores the possibility of intra-step absorption and thus, underestimates the number of absorbed molecules. The SMC algorithm is presented in **Algorithm 1**.

- As per the determination criterion in [6], a molecule is absorbed if the line segment from its initial position to its final position in the current simulation time step crosses the RX's boundary. However, we note that the line segment crossing the RX's surface is neither sufficient nor necessary to correctly detect intra-step absorption. For example, in Fig. 3.4, the molecule absorption that actually occurs cannot be detected by the criterion in [6]. In another case, shown in Fig. 4.1, molecule absorption is determined by the criterion in [6] but does not actually occur. The accuracy of the algorithm in [6] is better than but still comparable to the SMC algorithm. This algorithm is presented in **Algorithm 2**.

- As per the determination criterion in [5], referred to as the RMC algorithm and described in **Algorithm 3**, (3.21) is used to calculate the intra-step absorption probability for an RX with a perfectly absorbing spherical boundary. As depicted in Fig. 3.6, in the RMC algorithm, $l_{j\mathrm{i}}$ denotes the shortest distance between the jth molecule's initial position in the current simulation time step and the RX's boundary and $l_{j\mathrm{f}}$ denotes the shortest distance between the jth molecule's final position in the current time step and the RX's boundary. As shown in [5], the accuracy of the SMC algorithm is comparable to that of the RMC algorithm when Δt is relatively small. When Δt increases while other

parameters remain the same, the accuracy of the RMC algorithm becomes measurably higher than that of the SMC algorithm. However, in addition to the results presented in [5], we run simulations of the SMC and RMC algorithms and observe that the simulated fraction of absorbed molecules of the RMC algorithm deviates from the analytical one when the root mean square (RMS) of the diffusion step length, $\sqrt{2D\Delta t}$, is relatively larger than r_{r}. We will show the impact of the RMS of the diffusion step length on the accuracy of the RMC algorithm in Chapter 5.

Table 4.1: Comparison of Simulation Algorithms

Algorithm	Diffusion first?	Intra-step absorption?
SMC [9, 63]	Yes	No
RMC [5]	Yes	Yes. Absorption probability is given by (3.21).
AcCoRD [6]	Yes	Yes. Absorption occurs when the molecule trajectory crosses the RX's boundary.
APMC	No	No. Molecules are absorbed before being diffused.

4.1.2 Algorithm description

The algorithms discussed in this chapter are summarized in Table 4.1 and presented as follows.

Algorithm 1 The simplified Monte Carlo (SMC) algorithm

```
1: Determine the end time of simulation.
2: for all simulation time steps do
3:     if t = 0 then
4:         Add N molecules to environment.
5:     end if
6:     Scan all not-yet-absorbed molecules, i.e., molecules which are not absorbed
   by the RX.
7:     for all not-yet-absorbed molecules do
8:         Propagate each molecule for one step according to Brownian motion.
9:         if The molecule's current observed position is inside the RX, then
10:            The molecule is absorbed.
11:        end if
12:    end for
13: end for
```

Algorithm 2 The algorithm introduced in [6]

```
1: Determine the end time of simulation.
2: for all simulation time steps do
3:     if t = 0 then
4:         Add N molecules to environment.
5:     end if
6:     Scan all not-yet-absorbed molecules.
7:     for all not-yet-absorbed molecules do
8:         Propagate each molecule for one step according to Brownian motion.
9:         if The line segment from the molecule's previous observed location to its
   current observed location intersects the RX sphere, then
10:            The molecule is absorbed.
11:        end if
12:    end for
13: end for
```

Algorithm 3 The refined Monte Carlo (RMC) algorithm

```
Determine the end time of simulation.
for all simulation time steps do
    if t = 0 then
        Add N molecules to environment.
    end if
    Scan all not-yet-absorbed molecules.
    for all not-yet-absorbed molecules do
        Propagate each molecule for one step according to Brownian motion.
        if The molecule's current observed position is inside the RX, then
            The molecule is absorbed.
        else
            Calculate the intra-step absorption probability Pr_RMC using (3.21).
            if Pr_RMC ≥ u then                    ▷ u is a generated uniform RV.
                The molecule is absorbed.
            end if
        end if
    end for
end for
```

4.2 Performance Prediction of RMC Algorithm

In this section, we propose a rule-of-thumb expression to predict the accuracy of the RMC algorithm when the parameters of the MC system are within specified ranges. Specifically, our aim is to make a rough but fast prediction of the algorithm's accuracy for given parameters, without resorting to simulations.

Table 4.2: Range of MC System Parameters for Performance Prediction

Parameter	**Notation and Range**
TX-RX distance	$20\,\mu\text{m} \leq r_0 \leq 100\,\mu\text{m}$
Radius of RX	$0\,\mu\text{m} < r_\text{r} \leq r_0\,\mu\text{m}$
RMS of diffusion step length	$40\,\mu\text{m} \leq \sqrt{2D\Delta t} \leq \sqrt{20000}\,\mu\text{m}$
Accuracy	$R^2 \in \{0.6, 0.65, 0.7, 0.75, 0.8, 0.85, 0.9, 0.95, 0.99\}$

4.2.1 Empirical results

In this subsection, we describe the procedure that we follow to collect the empirical results on the accuracy of the RMC algorithm. The steps are shown as follows:

1. For the parameters listed in Table 4.2, we run simulations using the RMC algorithm for one time step. We note that the fraction of molecules absorbed at every current time step is based on the results generated in the previous time step, e.g., if all molecules are absorbed in the previous simulation time step, there will be no absorption in the next step. In order to eliminate the significant impact of results from previous time steps, we choose to test for the first simulation time step only. Simulation is repeated for N molecules and the result obtained from the simulation of each molecule is called a realization.

2. For each set of choices for D, Δt, and r_0, we plot R^2 versus r_r, where the measure of accuracy, R^2, is calculated according to

$$R^2 = 1 - \frac{\sum_{i=1}^{2} \left(\mathrm{Pr}_{\mathrm{RX}}\left(i-1\right) - \mathrm{Pr}_{\mathrm{sim}}\left(i-1\right)\right)^2}{\sum_{i=1}^{2} \left(\mathrm{Pr}_{\mathrm{sim}}\left(i-1\right) - \overline{\mathrm{Pr}}_{\mathrm{sim}}\right)^2}, \tag{4.1}$$

   where

$$\mathrm{Pr}_{\mathrm{RX}}(i-1) = \frac{N_{\mathrm{RX}}\left(\Omega_\mathrm{r}, (i-1)\Delta t | r_0\right)}{N} \tag{4.2}$$

   is the analytical fraction of absorbed molecules at time $(i-1)\Delta t$, as obtained from (3.1). We define $\mathrm{Pr}_{\mathrm{sim}}(i-1)$ as the simulated fraction of absorbed molecules at time $(i-1)\Delta t$, which is obtained by averaging the total number of absorbed molecules out of all realizations at $(i-1)\Delta t$ over N, and we refer to it as the ith simulated sample. Additionally, we define $\overline{\mathrm{Pr}}_{\mathrm{sim}}$ as the mean of all simulated samples. As we take samples only for the first simulation step, there are two samples in total, one at the beginning and another at the end of the first simulation time step.

3. We plot reference lines that indicate different values of R^2 in the same figures where we plot R^2 versus r_r. We denote M as the number of time-varying samples, and $M-1$ as the number of simulation time steps. An example of the plot is presented in Fig. 4.2, where we plot accuracy R^2 versus r_r for $N = 10^6$, $M = 2$, $D = 10^{-9}\,\mathrm{m^2/s}$, $r_0 = 50\,\mu\mathrm{m}$, and $\Delta t = 0.5\,\mathrm{s}$ or $\Delta t = 5\,\mathrm{s}$.

4. We observe the values of r_r, r_0, D, and Δt that achieve the R^2 in Table 4.2. To be specific, the r_r of every intersection point where the reference lines and the accuracy R^2 curve cross in the plots as well as the r_0, D, and Δt used for corresponding plots are recorded.

5. For each selected value of R^2, we use the collected parameters set to plot a 3D figure for curve fitting.

6. We further plot Figs. 4.3 and 4.4 to observe the changes in R^2 when varying other parameters other than r_r. In Fig. 4.3, we plot R^2 versus r_0 for $N = 10^6$, $M = 2$, $D = 10^{-9}\,\mathrm{m}^2/\mathrm{s}$, $\Delta t = 2\,\mathrm{s}$, and $r_\mathrm{r} = 10\,\mu\mathrm{m}$ or $r_\mathrm{r} = 20\,\mu\mathrm{m}$. In Fig. 4.4, we plot R^2 versus $D\Delta t$ for $N = 10^6$, $M = 2$, $r_0 = 50\,\mu\mathrm{m}$, and $r_\mathrm{r} = 10\,\mu\mathrm{m}$ or $r_\mathrm{r} = 30\,\mu\mathrm{m}$. We observe that generally, R^2 increases when r_r increases, R^2 decreases when r_0 increases, and that R^2 decreases when $D\Delta t$ increases.

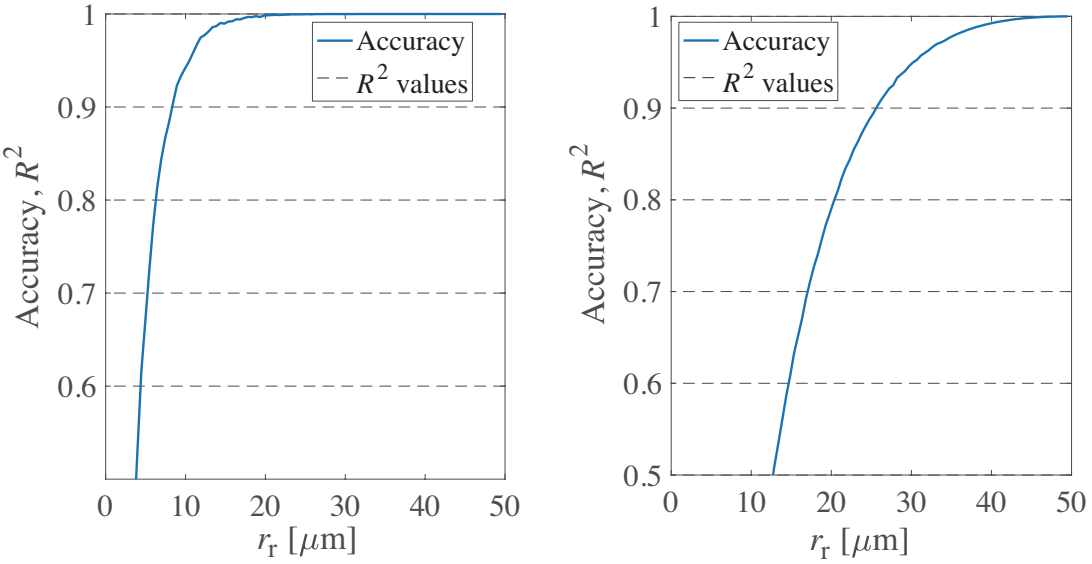

(a) $\Delta t = 0.5\,\mathrm{s}$ (b) $\Delta t = 5\,\mathrm{s}$

Figure 4.2: The accuracy of the RMC algorithm is plotted together with reference lines that indicate different R^2 versus r_r for $r_0 = 50\,\mu\mathrm{m}$, $N = 10^6$, $M = 2$, $D = 10^{-9}\,\mathrm{m}^2/\mathrm{s}$, and $\Delta t = 0.5\,\mathrm{s}$ or $\Delta t = 5\,\mathrm{s}$.

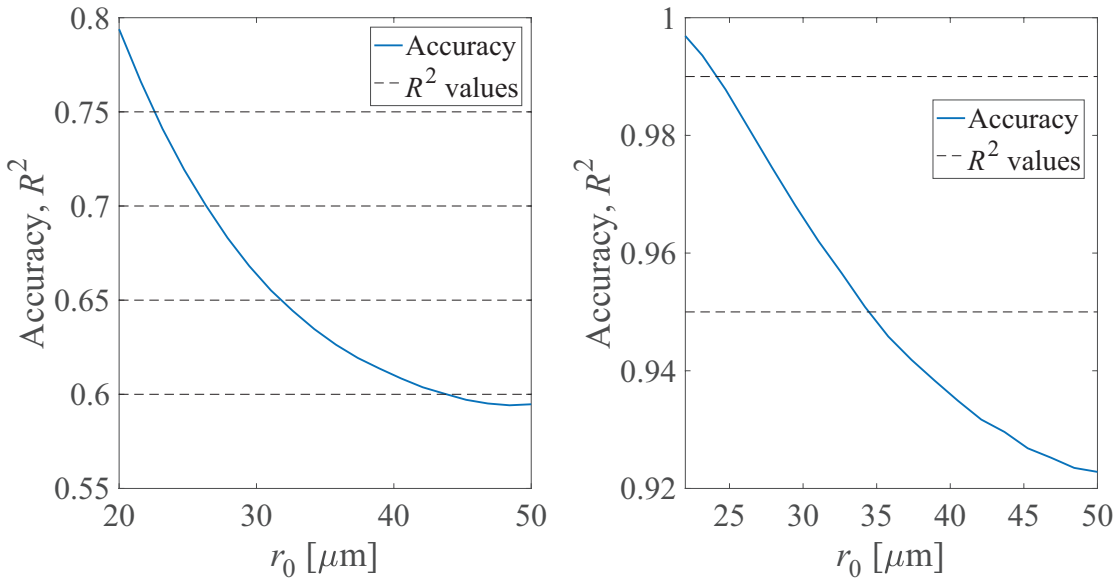

(a) $r_\mathrm{r} = 10\,\mu m$ (b) $r_\mathrm{r} = 20\,\mu m$

Figure 4.3: The accuracy of the RMC algorithm is plotted together with reference lines that indicate different R^2 versus r_0 for $N = 10^6$, $M = 2$, $D = 10^{-9}\,\mathrm{m}^2/\mathrm{s}$, $\Delta t = 2\,\mathrm{s}$, and $r_\mathrm{r} = 10\,\mu\mathrm{m}$ or $r_\mathrm{r} = 20\,\mu\mathrm{m}$.

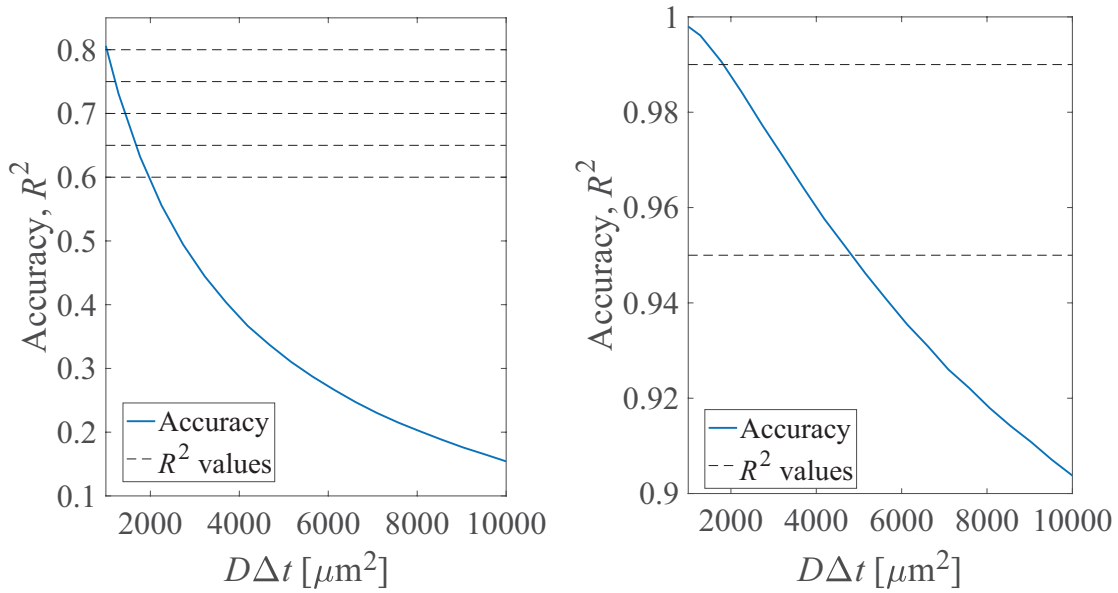

(a) $r_\mathrm{r} = 10\,\mu m$ (b) $r_\mathrm{r} = 30\,\mu m$

Figure 4.4: The accuracy of the RMC algorithm is plotted together with reference lines that indicate different R^2 versus $D\Delta t$ for $N = 10^6$, $M = 2$, $r_0 = 50\,\mu\mathrm{m}$, and $r_\mathrm{r} = 10\,\mu\mathrm{m}$ or $r_\mathrm{r} = 30\,\mu\mathrm{m}$.

4.2.2 3D curve fitting

We use the curve fitting tool in MATLAB to plot 3D figures with our collected data. The z-coordinate of the 3D figure is the recorded value of r_{r}, the x-coordinate is the recorded value of $D\Delta t$, and the y-coordinate is the recorded value of r_0. For each concerned R^2 value, we plot a subfigure. The eight subfigures in Figs. 4.5 and 4.6 plot the collected data and the polynomial fit surfaces given by the curve fitting tool in MATLAB for $R^2 = \{0.95, 0.9, 0.85, 0.8, 0.75, 0.7, 0.65, 0.6\}$, respectively.

To predict the accuracy, we define a dimensionless variable κ that is calculated from the simulation parameters of a MC system. Here, we define κ as

$$\kappa = r_{\mathrm{r}} \left(r_0 D\Delta t\right)^{-\frac{1}{3}}, \tag{4.3}$$

where the exponent of $-\frac{1}{3}$ is chosen such that the right hand side of the expression is dimensionless. This model is based on our observations from Figs. 4.2, 4.3, and 4.4. The exponents for each variable in (4.3) is chosen so that the measured RMS error (RMSE) of the difference between the fitting model and the collected data is minimized for all considered R^2.

Using the curve fitting tool, we obtain a set of best fit values for κ, as shown in the subcaption of each subfigure.

4.2.3 Polynomial fits for prediction

Next, we fit R^2 to a polynomial function of the obtained values of κ. We test the first, second, and third order polynomial fits, which are given by

$$R^2 \approx \frac{101\kappa + 47}{100}, \tag{4.4}$$

$$R^2 \approx \frac{-372\kappa^2 + 392\kappa - 3}{100}, \tag{4.5}$$

and

$$R^2 \approx \frac{979\kappa^3 - 1523\kappa^2 + 813\kappa - 51}{100}, \tag{4.6}$$

respectively. We do not test higher order fits in this thesis because we seek an easy-to-compute expression.

We will demonstrate in Chapter 5 that the third order polynomial fit is the best match among (4.4), (4.5), and (4.7). The accuracy of the three polynomial fits will be shown in Fig. 5.8 and the corresponding RMSE will be shown in Table 5.1.

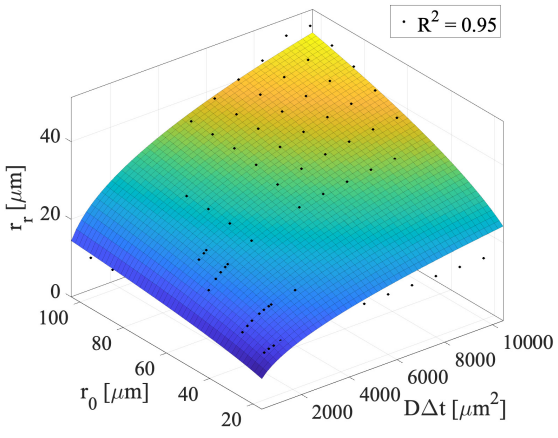

(a) $R^2 = 0.95, \kappa = 0.4405$.

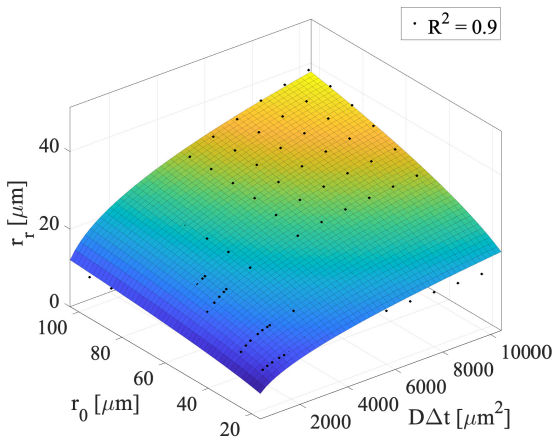

(b) $R^2 = 0.9, \kappa = 0.3672$.

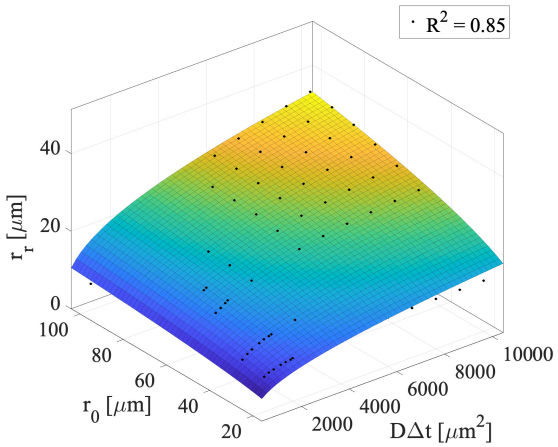

(c) $R^2 = 0.85, \kappa = 0.3220$.

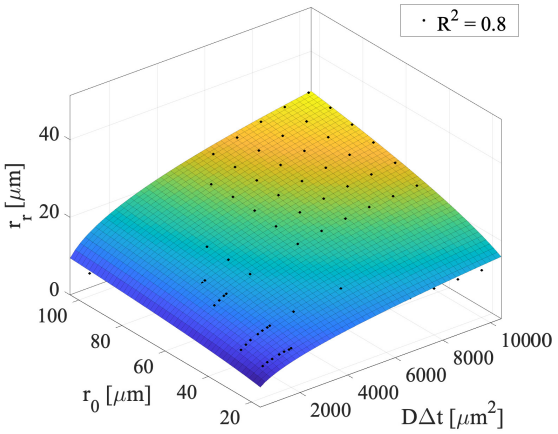

(d) $R^2 = 0.8, \kappa = 0.2890$.

Figure 4.5: 3D curve fitting plots of $r_r, r_0, D\Delta t$ values that achieve different R^2. The corresponding κ is given by the curve fitting tool in MATLAB.

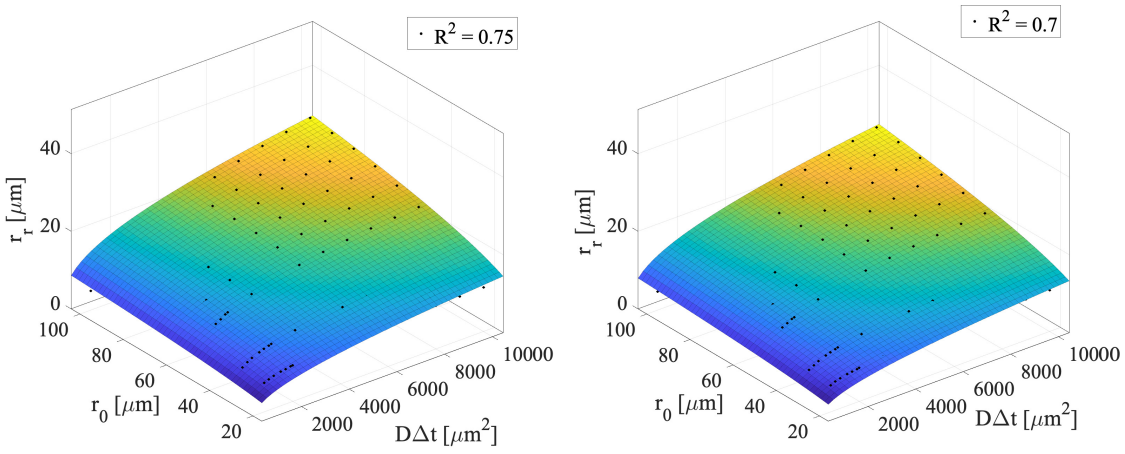

(a) $R^2 = 0.75, \kappa = 0.2630$.

(b) $R^2 = 0.7, \kappa = 0.2413$.

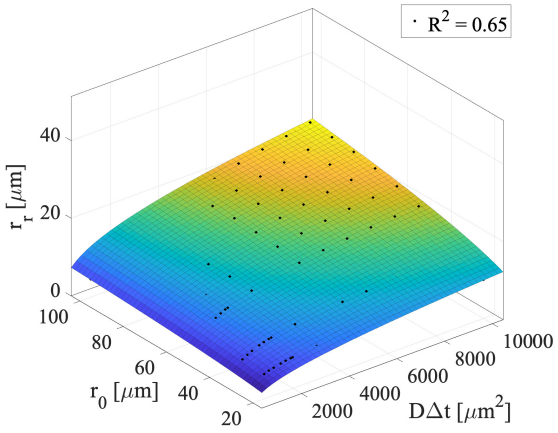

(c) $R^2 = 0.65, \kappa = 0.2227$.

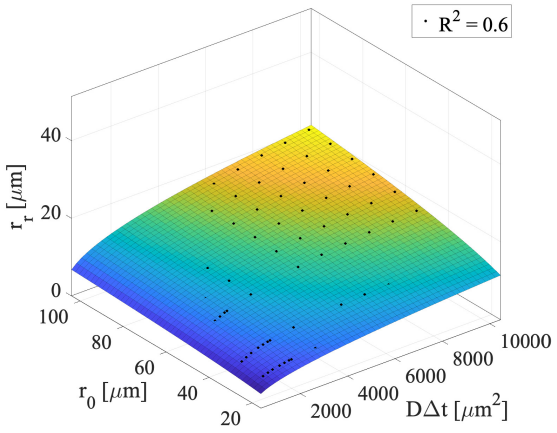

(d) $R^2 = 0.6, \kappa = 0.2067$.

Figure 4.6: Another set of 3D curve fitting plots of $r_r, r_0, D\Delta t$ values that achieve different R^2. The corresponding κ is given by the curve fitting tool in MATLAB.

Given that R^2 is a measure of accuracy, which implies $0 \leq R^2 \leq 1$, we impose $0.0726 \leq \kappa \leq 0.612$ for (4.6). If $\kappa > 0.612$, the RMC algorithm is predicted to have asymptotically high accuracy. If $\kappa < 0.0726$, then the RMC is predicted to have asymptotically low accuracy. Finally, we arrive at

$$R^2 \approx \begin{cases} 0, & \text{if } \kappa < 0.0726, \\ \dfrac{979\kappa^3 - 1523\kappa^2 + 813\kappa - 51}{100}, & \text{if } 0.0726 \leq \kappa \leq 0.612, \\ 1, & \text{otherwise.} \end{cases} \tag{4.7}$$

And (4.7) is the prediction expression we desire.

4.3 New *A Priori* Monte Carlo Algorithm

In this section, we propose a new simulation algorithm for approximating the fraction of molecules absorbed at a single perfectly absorbing RX in a diffusion-based MC system when $\sqrt{D\Delta t}/r_{\mathrm{r}}$ is larger than that considered for the RMC algorithm in [5]. We refer to the newly proposed algorithm as the APMC algorithm.

4.3.1 Formulation of the *a priori* probability

The procedure of the APMC algorithm is to first calculate, *before* the jth molecule diffuses, the probability that this molecule *will be* absorbed in the *current* simulation time step. This probability depends on the RX radius r_{r}, the diffusion coefficient D, the distance between the jth molecule's current location and the center of the RX d_j, and the simulation time step length Δt. Specifically, this probability is calculated as

$$\mathrm{Pr}_{\mathrm{APMC}} = \frac{r_{\mathrm{r}}}{d_j}\mathrm{erfc}\left(\frac{d_j - r_{\mathrm{r}}}{\sqrt{4D\Delta t}}\right), \tag{4.8}$$

which is obtained by scaling (3.1) by N, replacing the total simulation time t with Δt, and replacing r_0 with d_j. In (4.8), $\mathrm{Pr}_{\mathrm{APMC}}$ denotes the fraction of absorbed molecules released from a location d_j away from the RX at time $t_0 = 0\,\mathrm{s}$ and absorbed by the RX by time Δt. We note that (4.8) is calculated repeatedly in every time step for each of the free molecules with the molecule's current updated location when it diffuses. Then the molecule absorption is determined by generating a uniform RV u, where $0 \leq u \leq 1$, and comparing its value with the absorption probability obtained by (4.8). A molecule is marked as "absorbed" if $u \leq \mathrm{Pr}_{\mathrm{APMC}}$. After determining the molecules absorbed, each not-yet-absorbed molecule is propagated according to

Brownian motion. If any propagated molecule is inside the RX's boundary at the end of the current simulation time step, we *revert* the diffusion of this molecule and let it propagate again, until this molecule diffuses to a location outside the RX. This is because if a molecule propagates to a location inside the RX, it contradicts the preconditioning that the molecule is not absorbed. The APMC algorithm is detailed in **Algorithm 4**.

Algorithm 4 The APMC algorithm for molecule absorption

Determine the end time of simulation.
for all simulation time steps **do**
    if $t = 0$ **then**
        Release N molecules into environment.
    end if
    Scan all *not-yet-absorbed* molecules.
    for all *not-yet-absorbed* molecules **do**
        Calculate the distance between the jth molecule to $(r_0, 0, 0)$, denote by d_j.
        Calculate the absorbed probability $\Pr_{\text{APMC}}$ for the jth molecule using (4.8) with r_{r}, d_j, D, and Δt.
        if $\Pr_{\text{APMC}} \geq u$ **then** ▷ u is a generated uniform RV.
            The molecule is absorbed.
        end if
    end for
    for all *not-yet-absorbed* molecules **do**
        Propagate the molecule for one step.
        while The molecule's current observed position is inside the RX, **do**
            Revert the movement of this molecule to the location before propagation.
            Propagate this molecule for one step.
        end while
    end for
end for

4.4 Likelihood Threshold

4.4.1 Computational complexity analysis

In this subsection, we propose a likelihood threshold to reduce the computational complexity for the RMC algorithm and the APMC algorithm. For both algorithms, the computational complexity consists of three parts and can be written as

$$\mathcal{C}_{\text{sim}} = \mathcal{O}\left(\frac{t_{\text{end}}}{\Delta t}\left(c_{\text{diffuse}} + c_{\text{absorb}} + c_{\text{locate}}\right)\right), \tag{4.9}$$

where c_{diffuse} denotes the complexity of diffusing all molecules, c_{absorb} denotes the complexity of determining the molecules to be absorbed and absorbing these molecules, and c_{locate} denotes the complexity of determining whether a molecule is inside the spherical RX.

We observe from MATLAB run time profiles that the time for generating uniform RVs alone can take up around 10% of the total simulation run time of both algorithms and that an increase in the number of generated RVs is closely related to an increase in the total MATLAB simulation run time for both algorithms. Therefore, we use the number of generated RVs to characterize the computational complexity of both algorithms.

4.4.2 Conversion from Gaussian RVs to uniform RVs

There are two types of generated RVs for the APMC algorithm and the RMC algorithm, namely, the uniform RVs used for testing the molecule absorptions and the Gaussian RVs used for propagating molecules according to Brownian motion. Thus, we denote $\mathcal{N}_{\text{u}}$ and $\mathcal{N}_{\text{g}}$ as the number of generated uniform RVs and the number of generated Gaussian RVs, respectively.

For each determination of molecule absorption, as shown in Line 13 in **Algorithm 3** and Line 10 in **Algorithm 4**, we add 1 to $\mathcal{N}_{\text{u}}$. For each molecule propagation, as shown in Line 8 in **Algorithm 1** and Lines 15 and 18 in **Algorithm 4**, we add 3 to $\mathcal{N}_{\text{g}}$ since there are three Gaussian RVs added to the x-, y-, and z-coordinates of a molecule.

Here, we adopt the commonly used Box-Muller transform [64] to convert the number of generated Gaussian RVs to an equivalent number of generated uniform RVs. According to [64], the generation of a pair of Gaussian RVs requires $4/\pi$ pairs of

uniform RVs. Thus, we use $4/\pi$ as a conversion factor and then the equivalent number of totally generated uniform RVs, which characterizes the computational complexity of simulation, is given by $\mathcal{N}_{\text{total}} = \mathcal{N}_{\text{u}} + (4/\pi)\mathcal{N}_{\text{g}}$.

Based on the aforementioned computational complexity characterization, we now apply a likelihood threshold, ξ, to ignore the calculated absorption probabilities that are lower than ξ. With this likelihood threshold, the intra-step absorption for the RMC algorithm is possible if and only if $\text{Pr}_{\text{RMC}} \geq \xi$, while the *a priori* molecule absorption for the APMC algorithm is possible if and only if $\text{Pr}_{\text{APMC}} \geq \xi$. This can significantly reduce $\mathcal{N}_{\text{u}}$ in simulation. Although the accuracy of the RMC and APMC algorithms may slightly decrease when ξ applies, an appropriate value of ξ can provide a good trade-off between simulation accuracy and computational complexity. Such trade-off of the RMC and APMC algorithms will be illustrated in Chapter 5.

The value of ξ is determined by running test simulations first using the same system parameters, but for a much shorter communication time than the actual one. Then we apply a range of thresholds to find the value of ξ that is desirable in terms of both accuracy and computational complexity for the test simulations. After this, the determined ξ can be applied in the full simulation.

4.5 Simulation for Multiple Absorbing Receivers

In this section, we describe the modified RMC and APMC algorithms in the simulation of multiple perfectly absorbing RXs in a diffusion-based MC system.

4.5.1 Simulation using the RMC algorithm

With multiple RXs in the system, the intra-step absorption probability of a molecule with each RX in a simulation time step is calculated individually. Then the RX that has the highest probability of absorbing the molecule is selected to proceed with generating the uniform RV and comparing the uniform RV with the intra-step absorption probability. If the RX that has the highest probability of absorbing the molecule is determined as will not absorb the molecule, then the molecule will not be absorbed by other RXs. This method ensures that a molecule will only be absorbed by one of the RXs. The modified algorithm is shown in **Algorithm 5**.

Algorithm 5 The RMC algorithm for molecule absorption in a two-RX system

Determine the end time of simulation.
for all simulation time steps **do**
    if $t = 0$ **then**
        Add N molecules to environment.
    end if
    Scan all *not-yet-absorbed* molecules.
    for all *not-yet-absorbed* molecules **do**
        Propagate each molecule for one step according to Brownian motion.
        if The molecule's current observed position is inside any of the RXs, **then**
            The molecule is absorbed.
        else
            Calculate the intra-step absorption probabilities for the molecule with each of the RXs, using (3.21).
            Find the highest value of the calculated intra-step absorption probabilities.
            if the highest value of the calculated $\Pr_{\text{RMC}} \geq u$ **then** ▷ u is a generated uniform RV.
                The molecule is absorbed by the RX that has the the highest value of the calculated intra-step absorption probability.
            end if
        end if
    end for
end for

4.5.2 Simulation using the APMC algorithm

Similarly, the *a priori* probability of every molecule with each RX in a simulation time step is calculated individually for the APMC algorithm when simulating diffusion-based MC systems with multiple perfectly absorbing RXs. The RX that has the highest *a priori* probability is selected to proceed with generating a uniform RV and comparing the uniform RV with the *a priori* probability. If the RX that has the highest *a priori* probability is determined as will not absorb the molecule, then the molecule will not be absorbed by other RXs. The modified algorithm is shown in **Algorithm 6**.

Algorithm 6 The APMC algorithm for molecule absorption in a two-RX system

Determine the end time of simulation.
for all simulation time steps **do**
    if $t = 0$ **then**
        Release N molecules into environment.
    end if
    Scan all *not-yet-absorbed* molecules.
    for all *not-yet-absorbed* molecules **do**
        Calculate the absorbed probability for the molecule with each of the RXs using (4.8).
        Find the highest one of the calculated *a priori* absorption probabilities.
        if the highest value of the calculated $\Pr_{\text{APMC}} \geq u$ **then** ▷ u is a generated uniform RV.
            The molecule is absorbed by the RX that has the highest *a priori* absorption probability.
        end if
    end for
    for all *not-yet-absorbed* molecules **do**
        Propagate the molecule for one step.
        while The molecule's current observed position is inside any of the RXs **do**
            Revert the movement of this molecule to the location before propagation.
            Propagate this molecule for one step.
        end while
    end for
end for

Chapter 5

Numerical Results and Discussions

In this chapter, we present the results of our numerical simulations. The algorithms are implemented in MATLAB. We first compare the time-varying fraction of molecules absorbed determined by the SMC algorithm, the RMC algorithm, and the APMC algorithm, with the aid of particle-based simulations, to show the benefits of our APMC algorithm. We also investigate the performance of the prediction expression obtained from empirical simulations in Section 4.2. Furthermore, we compare MATLAB simulation run times of the RMC and APMC algorithms and explore the trade-off between simulation accuracy and computational complexity of algorithms.

5.1 System Parameters and Measurements

We state the system parameters used for each figure in the caption. We recall from previous chapters that M is the number of time-varying samples in a single transmission, $M-1$ is the number of simulation time steps, N is the number of molecules released for each transmission, Δt is the simulation time step length, D is the diffusion coefficient, r_{r} is the radius of RX, r_0 is the TX-RX distance for the investigated systems and ξ is the likelihood threshold for absorption probabilities. We also recall that R^2 is the main measure of accuracy used throughout this thesis, which is calculated by (4.1).

5.2 Time-Varying Received Signal

5.2.1 Received signal for a single absorbing receiver

We first examine the impact of r_{r} and Δt on the fraction of molecules absorbed produced by the algorithms in Fig. 5.1, Fig. 5.2, Fig. 5.3, and Fig. 5.4.

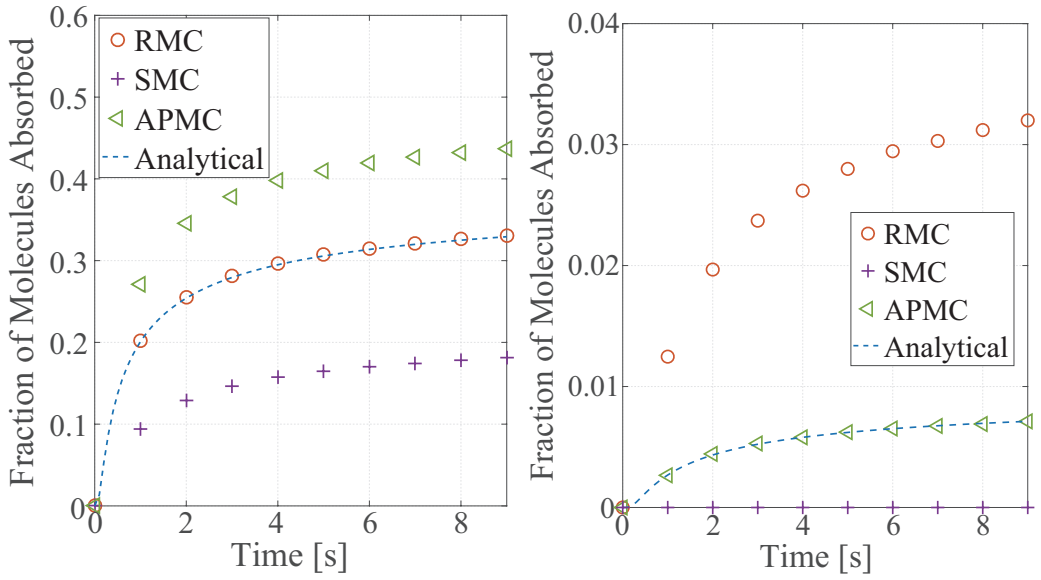

(a) $r_{\mathrm{r}} = 20\,\mu\mathrm{m}$ (b) $r_{\mathrm{r}} = 0.5\,\mu\mathrm{m}$

Figure 5.1: Comparison of the fraction of molecules absorbed produced by the SMC algorithm, the RMC algorithm, and the APMC algorithm versus time for $r_0 = 50\,\mu\mathrm{m}$, $N = 10^6$, $M = 100$, $D = 10^{-9}\,\mathrm{m}^2/\mathrm{s}$, $\Delta t = 0.1\,\mathrm{s}$, and $r_{\mathrm{r}} = 20\,\mu\mathrm{m}$ or $r_{\mathrm{r}} = 0.5\,\mu\mathrm{m}$.

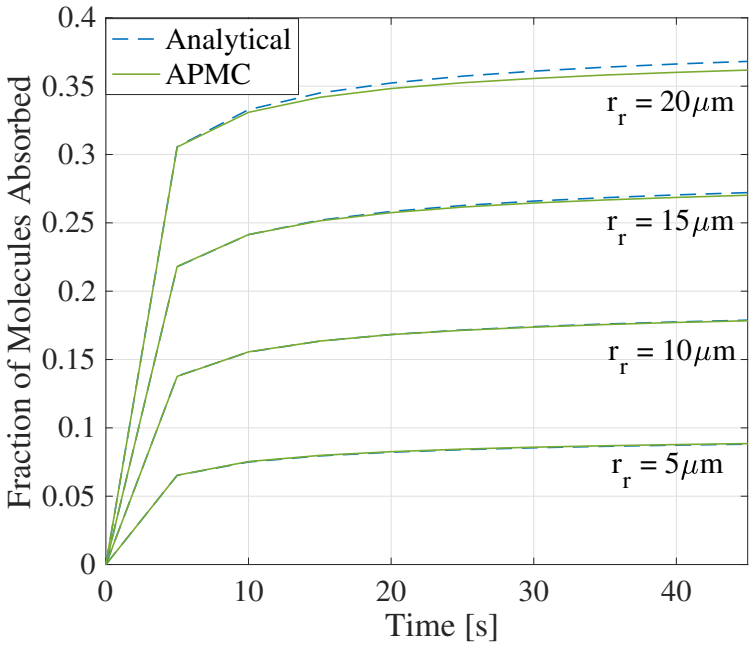

Figure 5.2: The fraction of molecules absorbed produced by the APMC algorithm versus time for $r_0 = 50\,\mu\mathrm{m}$, $N = 10^6$, $M = 10$, $D = 10^{-9}\,\mathrm{m}^2/\mathrm{s}$, $\Delta t = 5\,\mathrm{s}$, and $r_{\mathrm{r}} = \{5, 10, 15, 20\}\,\mu\mathrm{m}$.

Fig. 5.1 plots the simulated fraction of molecules absorbed versus time t for $r_0 = 50\,\mu\mathrm{m}$, $N = 10^6$, $M = 100$, $D = 10^{-9}\,\mathrm{m}^2/\mathrm{s}$, $\Delta t = 0.1\,\mathrm{s}$, and $r_{\mathrm{r}} = 20\,\mu\mathrm{m}$ or $r_{\mathrm{r}} = 0.5\,\mu\mathrm{m}$. In this figure, the analytical results obtained using (3.1) are also plotted for

examining the accuracy of the algorithms.

We observe from Fig. 5.1(a) that the SMC algorithm and the APMC algorithm underestimates and overestimates the fraction of molecules absorbed, respectively, for the considered set of parameters while the RMC algorithm matches the fraction of molecules absorbed as predicted by the analytical result. Different from Fig. 5.1(a), Fig. 5.1(b) shows that the APMC algorithm matches the fraction of molecules absorbed predicted by the analytical result while the other two algorithms do not. Particularly in Fig. 5.1(b), the fractions of molecules absorbed produced by the RMC and SMC algorithms are very far away from the analytical result when $t > 0\,\mathrm{s}$.

By comparing Fig. 5.1(a) and Fig. 5.1(b), we observe that when r_r is $20\,\mu\mathrm{m}$, the RMC algorithm matches the fraction of molecules absorbed as predicted by the analytical result while when r_r is $0.5\,\mu\mathrm{m}$, the RMC algorithm significantly overestimates the fraction of molecules absorbed as predicted by the analytical result, which meets our expectation. The performance of the RMC algorithm corresponds to the value of $\sqrt{D\Delta t}/r_\mathrm{r}$ because $\sqrt{D\Delta t}/r_\mathrm{r}$ compares the mean simulation diffusion step length with the radius of the RX. When $\sqrt{D\Delta t}/r_\mathrm{r}$ approaches 0 and r_0 is larger than r_r, the surface of the RX can be approximated by an infinite plane. Therefore, the probability of a molecule entering the spherical RX between time steps is comparable to the probability of a molecule crossing a flat planar boundary between time steps. When $\sqrt{D\Delta t}/r_\mathrm{r}$ is relatively large, the spherical RX's boundary cannot be approximated by a flat planar boundary. Therefore, the RMC algorithm overestimates the fraction of molecules absorbed a lot. Furthermore, we observe from Fig. 5.2 that when $r_0 = 50\,\mu\mathrm{m}$ and $\Delta t = 5\,\mathrm{s}$, our APMC algorithm matches the analytical result better when r_r decreases while other parameters remain unchanged. This figure demonstrates the advantage of our APMC algorithm in accuracy when Δt is large and $\sqrt{D\Delta t}/r_\mathrm{r}$ increases.

Fig. 5.3 plots the simulated fraction of molecules absorbed, together with the analytical result obtained using (3.1), versus time t for $r_0 = 50\,\mu\mathrm{m}$, $N = 10^6$, $M = 10$, $D = 10^{-9}\,\mathrm{m}^2/\mathrm{s}$, $r_\mathrm{r} = 10\,\mu\mathrm{m}$, and $\Delta t = 0.5\,\mathrm{s}$ or $\Delta t = 5\,\mathrm{s}$. We observe from this figure that when Δt increases from $0.5\,\mathrm{s}$ to $5\,\mathrm{s}$, our APMC algorithm achieves a higher accuracy. Specifically, Fig. 5.3(a) shows that the gap between the fraction of molecules absorbed produced by the APMC algorithm and that produced by the RMC algorithm is very small. Also, Fig. 5.3(a) shows that both the APMC and RMC algorithms overestimate the fraction of molecules absorbed and that the SMC algorithm significantly underestimates the analytical result. Unlike Fig. 5.3(a), Fig. 5.3(b) shows that the APMC algorithm matches the fraction of molecules ab-

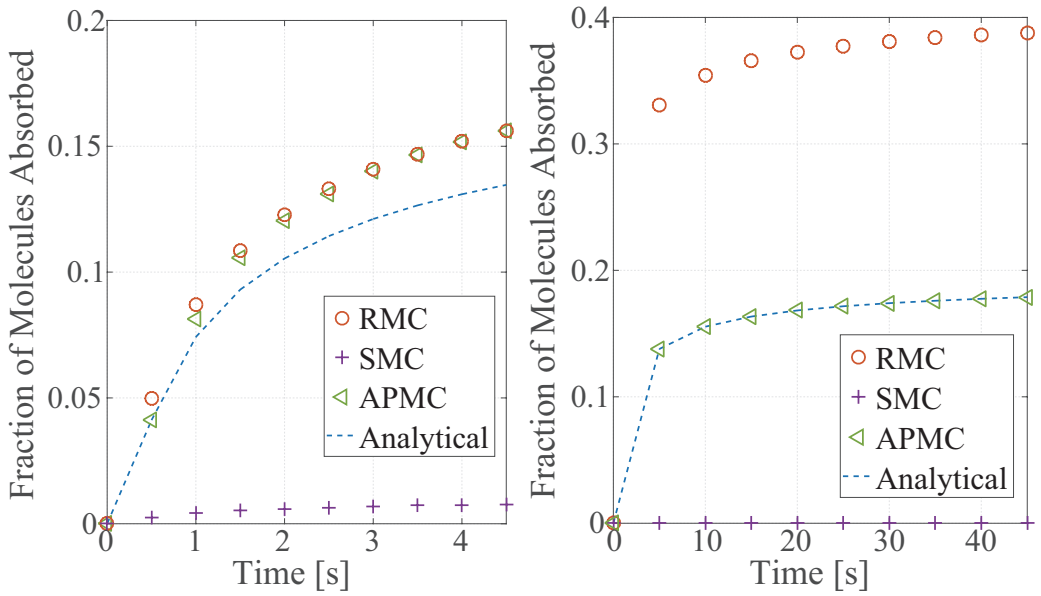

(a) $\Delta t = 0.5\,\mathrm{s}$ (b) $\Delta t = 5\,\mathrm{s}$

Figure 5.3: Comparison of the fraction of molecules absorbed results produced by the SMC algorithm, the RMC algorithm, and the APMC algorithm versus time for $r_0 = 50\,\mu\mathrm{m}$, $N = 10^6$, $M = 10$, $D = 10^{-9}\,\mathrm{m}^2/\mathrm{s}$, $r_\mathrm{r} = 10\,\mu\mathrm{m}$, and $\Delta t = 0.5\,\mathrm{s}$ or $\Delta t = 5\,\mathrm{s}$.

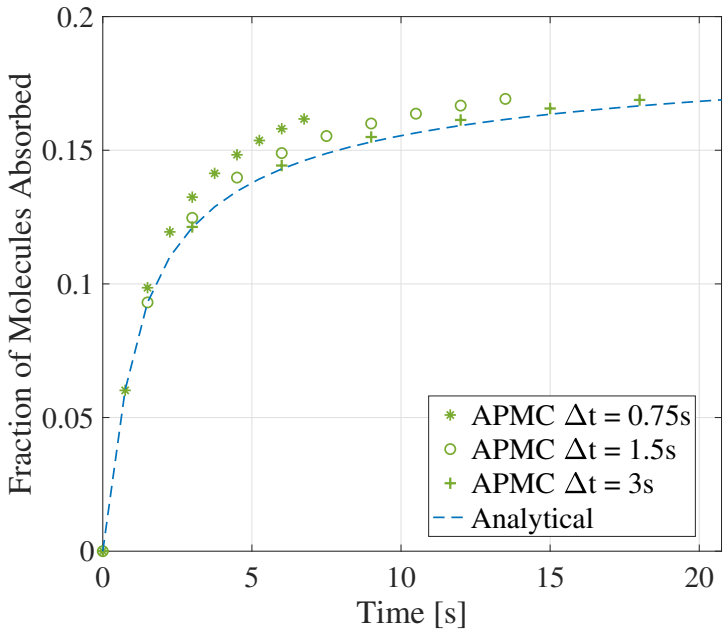

Figure 5.4: The fraction of molecules absorbed produced by the APMC algorithm versus time for $r_0 = 50\,\mu\mathrm{m}$, $N = 10^6$, $M = 10$, $D = 10^{-9}\,\mathrm{m}^2/\mathrm{s}$, $r_\mathrm{r} = 10\,\mu\mathrm{m}$, and $\Delta t = \{0.75, 1.5, 3\}\,\mathrm{s}$.

sorbed predicted by the analytical result while the RMC algorithm overestimates and the SMC algorithm underestimates the analytical result. The fraction of molecules absorbed produced by the RMC algorithm is approximately twice that produced by the APMC algorithm when $t > 0\,\mathrm{s}$ in Fig. 5.3(b). We further observe from Fig. 5.4

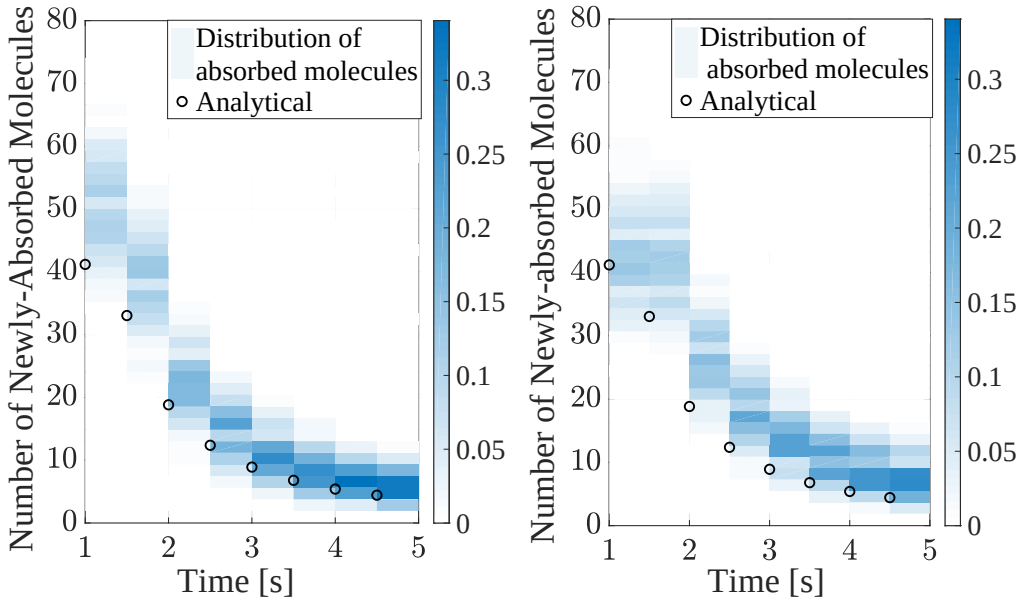

(a) RMC Algorithm (b) APMC Algorithm

Figure 5.5: Distribution of the number of newly-absorbed molecules during each time step for the RMC and APMC algorithms versus time for $r_0 = 50\,\mu$m, $N = 10^3$, $M = 10$, $D = 10^{-9}\,\mathrm{m}^2/\mathrm{s}$, $r_\mathrm{r} = 10\,\mu$m, and $\Delta t = 0.5\,$s. The spectrum bars represent observation probabilities.

that when $r_0 = 50\,\mu$m, $r_\mathrm{r} = 10\,\mu$m, and Δt increases while other parameters remain the same, our APMC algorithm produces more precise results, compared to the analytical ones. This again demonstrates that our APMC algorithm has a higher accuracy when $\sqrt{D\Delta t}/r_\mathrm{r}$ becomes large.

Fig. 5.5 depicts the distribution of newly-absorbed molecules during each simulation time step (e.g., from $t = 1\,$s to $t = 1.5\,$s) for both the RMC and APMC algorithms versus time t for $r_0 = 50\,\mu$m, $N = 10^3$, $M = 10$, $D = 10^{-9}\,\mathrm{m}^2/\mathrm{s}$, $r_\mathrm{r} = 10\,\mu$m, and $\Delta t = 0.5\,$s. The analytical result in this figure is obtained by first simulating using (3.1) and then calculating the differences between adjacent samples.

Comparing Fig. 5.5(a) with Fig. 5.5(b), we observe that the RMC algorithm significantly overestimates the number of newly-absorbed molecules when $t = 1\,$s, while our APMC algorithm gives an improved accuracy when $t = 1\,$s by absorbing molecules according to (4.8).

When t increases, the overestimation of the RMC algorithm becomes slightly less severe than that of the APMC algorithm, which is in accordance with the observation from Fig. 5.3(a). More importantly, we observe that the distribution of newly-absorbed molecules in Fig. 5.5(b) is very similar to that in Fig. 5.5(a), which demonstrates that our APMC algorithm does not noticeably disrupt the statistical

distribution of molecules.

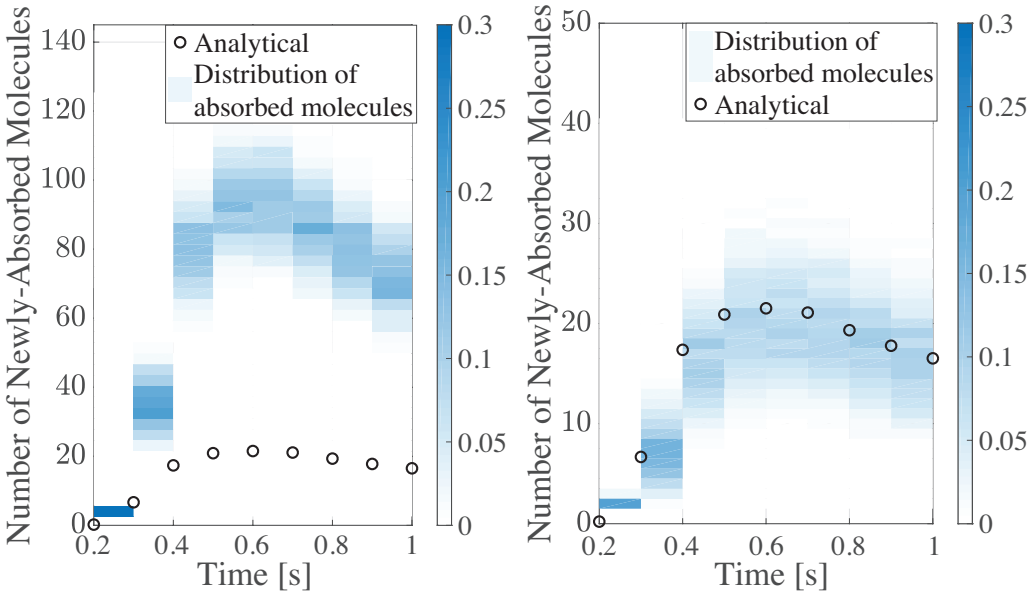

(a) RMC Algorithm (b) APMC Algorithm

Figure 5.6: Distribution of the number of newly-absorbed molecules during each time step for the RMC and APMC algorithms versus time for $r_0 = 50\,\mu$m, $N = 10^3$, $M = 10$, $D = 10^{-9}\,\mathrm{m}^2/\mathrm{s}$, $r_\mathrm{r} = 0.5\,\mu$m, and $\Delta t = 0.1\,$s. The spectrum bars represent observation probabilities.

Similarly, Fig. 5.6 plots the distribution of newly-absorbed molecules during each simulation time step for both algorithms versus time t for $r_0 = 50\,\mu$m, $N = 10^3$, $M = 10$, $D = 10^{-9}\,\mathrm{m}^2/\mathrm{s}$, $r_\mathrm{r} = 0.5\,\mu$m, and $\Delta t = 0.1\,$s. Comparing Fig. 5.6(a) with Fig. 5.6(b), we observe that the RMC algorithm significantly overestimates the number of newly-absorbed molecules when $t > 0.3\,$s, while the average number newly-absorbed molecules produced by the APMC algorithm matches well with the analytical distribution, which is shown in circles.

5.2.2 Received signal for multiple absorbing receivers

In this subsection, we focus on the MC system with multiple absorbing RXs. We run simulations for the system with two absorbing RXs, placed symmetrically as described in Chapter 3, and the system with four absorbing RXs, where the TX is a point located at the origin, and the RXs are located at $(r_0, 0, 0)$, $(-r_0, 0, 0)$, $(0, r_0, 0)$, and $(0, -r_0, 0)$ in a Cartesian coordinate system with the radius of all RXs set as r_r. For both systems, we examine the fraction of molecules absorbed as produced by the RMC and APMC algorithms. Due to symmetry of the systems, the probabilities that a molecule being absorbed by each of the RXs are identical.

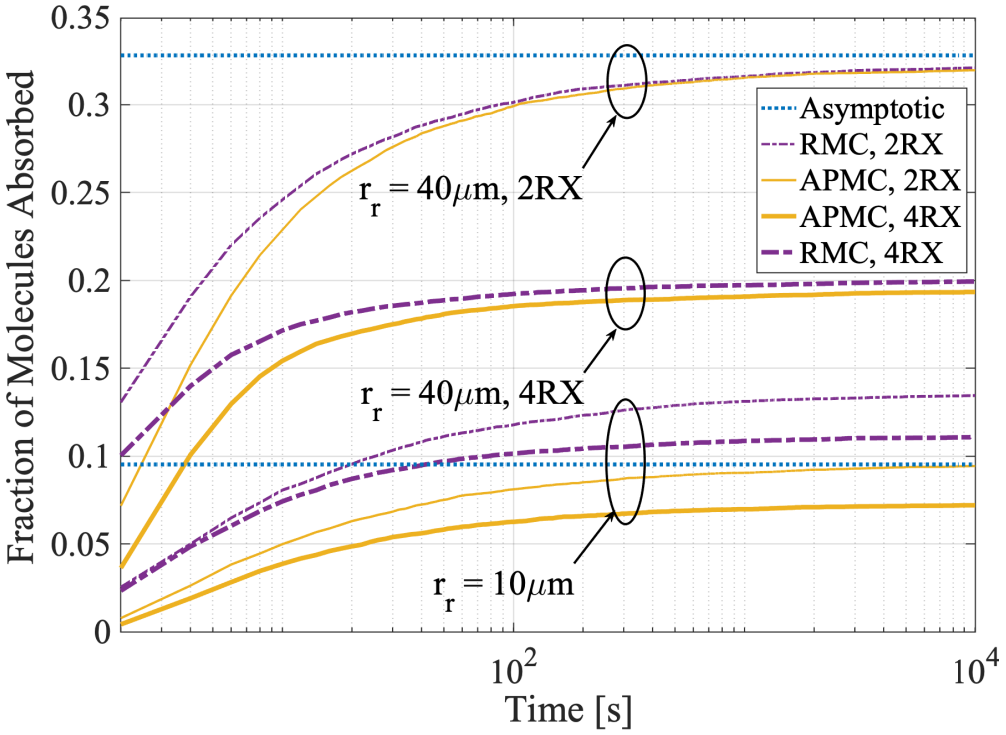

Figure 5.7: Comparison of the fraction of molecules absorbed for a system with two perfectly absorbing RXs and a system with four perfectly absorbing RXs. Results are produced by the RMC algorithm and the APMC algorithm versus time for $r_0 = 100\,\mu$m, $M = 5 \times 10^3$, $D = 1.05 \times 10^{-9}\,\mathrm{m}^2/\mathrm{s}$, $\Delta t = 2\,$s, with $r_\mathrm{r} = 10\,\mu$m and $r_\mathrm{r} = 40\,\mu$m. The asymptotic fraction of absorbed molecules of one of the RXs in a system with two perfectly absorbing RXs as time goes to infinity is also plotted.

Fig. 5.7 plots the simulated fraction of molecules absorbed by one of the RXs versus time t for $r_0 = 100\,\mu$m, $M = 5 \times 10^3$, $\Delta t = 2\,$s, and $r_\mathrm{r} = \{10, 40\}\,\mu$m for the system with two absorbing RXs and the system with four absorbing RXs. For the system with two absorbing RXs, we compare the simulated results with the asymptotic fractions of molecules absorbed calculated using (3.14) to examine the accuracy of simulations. This is due to a lack of time-varying analytical results for the fraction of molecules absorbed by two absorbing RXs in the literature. We observe that when $r_\mathrm{r} = 10\,\mu$m, the fraction of molecules absorbed as produced by the APMC algorithm approaches the asymptotic results when t is large, while the fraction of molecules absorbed as produced by the RMC algorithm is much higher than the asymptotic results. This is because when r_r is small, the spherical RX's boundary cannot be accurately approximated by a flat planar boundary. We also observe that when r_r increases to $40\,\mu$m, the fractions of molecules absorbed as produced by both algorithms approach the asymptotic results when t is large. Indeed, when r_r increases, the approximation of the spherical RX's boundary by a flat planar boundary becomes more accurate.

For the system with four absorbing RXs, we observe that when r_{r} increases to $40\,\mu$m, the fraction of molecules absorbed produced by the APMC algorithm approaches that produced by the RMC algorithm. This observation is similar to our observation of the system with two absorbing RXs.

5.3 Performance Prediction

We now examine the prediction expression for the RMC algorithm by comparing the predicted accuracy (without running the RMC algorithm) with the measured one (with running the RMC algorithm). The expressions for the first, second, and third order polynomial fits to predict accuracy are given by (4.4), (4.5), and (4.7), respectively in the previous chapter. We note that the calculation of (4.4), (4.5), and (4.7) requires κ only. As given by (4.3), κ is a function of D, Δt, r_0, and r_{r}.

Table 5.1: RMSE Measurements for Polynomial Fits in Fig. 5.8

	1st order fit	**2nd order fit**	**3rd order fit**
Fig. 5.8(a)	0.0638	0.1487	0.0440
Fig. 5.8(b)	0.0255	0.4378	0.0218

Fig. 5.8 plots the predicted accuracy of (4.4), (4.5), and (4.7) as well as the measured accuracy of the APMC and RMC algorithms versus $D\Delta t$ for $r_0 = 40\,\mu$m, $N = 10^6$, $M = 2$, and $r_{\mathrm{r}} = 15\,\mu$m, or $r_{\mathrm{r}} = 20\,\mu$m. We first observe from Fig. 5.8 that when $D\Delta t$ increases, for a fixed r_{r}, the measured accuracy of the RMC algorithm is at first higher than that of the APMC algorithm, but soon becomes much lower than that of the APMC algorithm. We also observe in both subfigures that the measured accuracy of the APMC algorithm stays close to 1 for most of the range of $D\Delta t$ considered. This demonstrates the accuracy and robustness of our APMC algorithm when $\sqrt{D\Delta t}/r_{\mathrm{r}}$ is large.

To quantitatively assess the performance of the first, second, and third order polynomial fits in Fig. 5.8, we calculate the RMSE measurements of these fits via

$$\mathrm{RMSE} = \sqrt{\frac{\sum_{i=1}^{2} \left(\mathrm{Pr}_{\mathrm{RX}}(i-1) - \mathrm{Pr}_{\mathrm{sim}}(i-1)\right)^2}{2}}, \tag{5.1}$$

where $\mathrm{Pr}_{\mathrm{RX}}(i-1)$, $\mathrm{Pr}_{\mathrm{sim}}(i-1)$, and i are defined the same as in (4.1).

The RMSE measurements for both subfigures are given in Table 5.1. Based on both subfigures and Table 5.1, we find that the third order polynomial fit for R^2

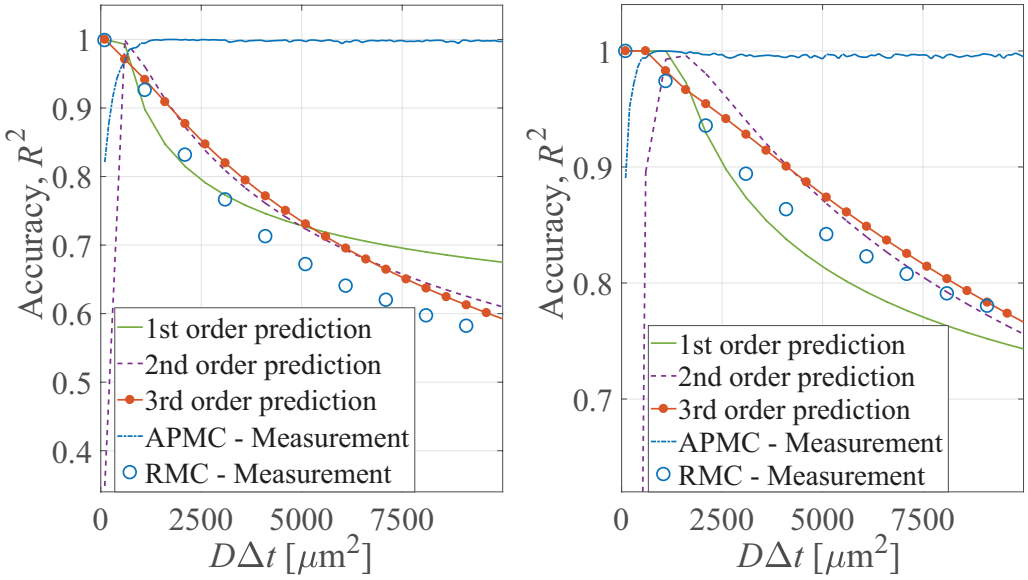

(a) $r_r = 15\,\mu$m (b) $r_r = 20\,\mu$m

Figure 5.8: Measured and predicted accuracy of the RMC algorithm and the measured accuracy of the APMC algorithm versus $D\Delta t$ for $r_0 = 40\,\mu$m, $N = 10^6$, $M = 2$, and $r_r = 15\,\mu$m, or $r_r = 20\,\mu$m.

is more accurate than the first and second order polynomial fits for $r_r = 15\,\mu$m and $20\,\mu$m, since the third order polynomial fit is, on average, the closest one to the measured accuracy, as shown in both subfigures, and achieves the lowest RMSE fitting measurement, as shown in Table 5.1. Therefore, in Figs. 5.9 and 5.10 we only consider the third order polynomial fit for the RMC algorithm.

Fig. 5.9 plots the measured accuracy and the predicted accuracy of the RMC algorithm versus $D\Delta t$ for $r_0 = 50\,\mu$m, $N = 10^6$, $M = 2$, with $r_r = 20\,\mu$m, $r_r = 25\,\mu$m, and $r_r = 30\,\mu$m. To calculate the measured accuracy at a given $D\Delta t$, we run simulations for different combinations of D and Δt which achieve the same $D\Delta t$, e.g., the combination of $D = 2 \times 10^{-9}\,\mathrm{m}^2/\mathrm{s}$ and $\Delta t = 0.5\,\mathrm{s}$ or the combination of $D = 1 \times 10^{-9}\,\mathrm{m}^2/\mathrm{s}$ and $\Delta t = 1\,\mathrm{s}$. The simulated result for each combination is displayed by a point (i.e., circle) in a scatter plot.

We observe that the points overlap with each other for a given $D\Delta t$, which demonstrates that the performance of the RMC algorithm depends on $D\Delta t$, but not D or Δt separately. We further find that the average absolute value of the difference between the measured accuracy and the predicted accuracy is 5.66% for $r_r = 20\,\mu$m, 3.27% for $r_r = 25\,\mu$m, and 1.45% for $r_r = 30\,\mu$m, all of which are lower than 6%.

Fig. 5.10 plots the measured and predicted accuracy of the RMC algorithm together with the measured accuracy of the APMC algorithm versus r_r for $r_0 = 80\,\mu$m, $N =$

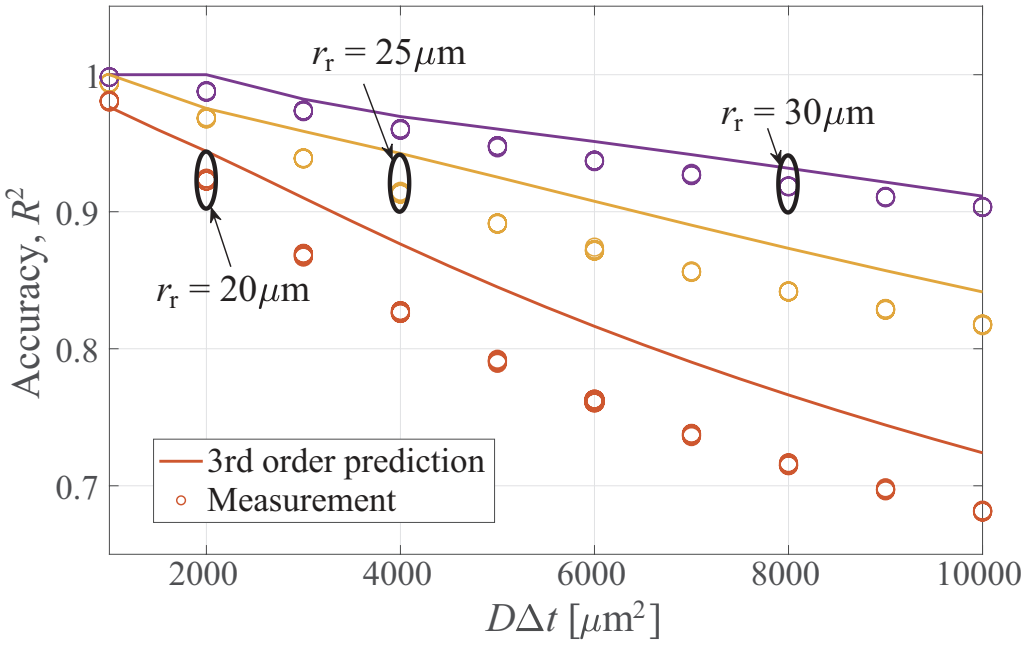

Figure 5.9: Measured and predicted accuracy of the RMC algorithm versus $D\Delta t$ for $r_0 = 50\,\mu$m, $N = 10^6$, $M = 2$, with $r_r = 20\,\mu$m, $r_r = 25\,\mu$m, and $r_r = 30\,\mu$m.

10^6, $M = 2$, $D = 10^{-9}\,\text{m}^2/\text{s}$, with large simulation time step lengths $\Delta t = 1\,\text{s}$ and $\Delta t = 3\,\text{s}$. As we observe from this figure, the accuracy of the APMC algorithm stays close to 1 for most of the range of r_r considered. This demonstrates that for large simulation time step lengths, the APMC algorithm preserves a very high accuracy, which agrees with the discussion on Fig. 5.3(b), and the variance in accuracy is small.

In addition, we observe that the measured accuracy of the RMC algorithm in Fig. 5.10 agrees well with the third order polynomial fit given in (4.7). This is in accordance with the observation made from Fig. 5.9 that the third order polynomial fit very well approximates the measured accuracy when $D\Delta t \leq 3000$.

5.4 Computational Complexity

As discussed earlier in this chapter, we have observed that when simulating with large time steps, the APMC algorithm stays accurate and has a much lower computational complexity than the RMC algorithm. In this section, we further explore the computation time of algorithms under the same Δt and explore the trade-off between simulation accuracy and computational complexity.

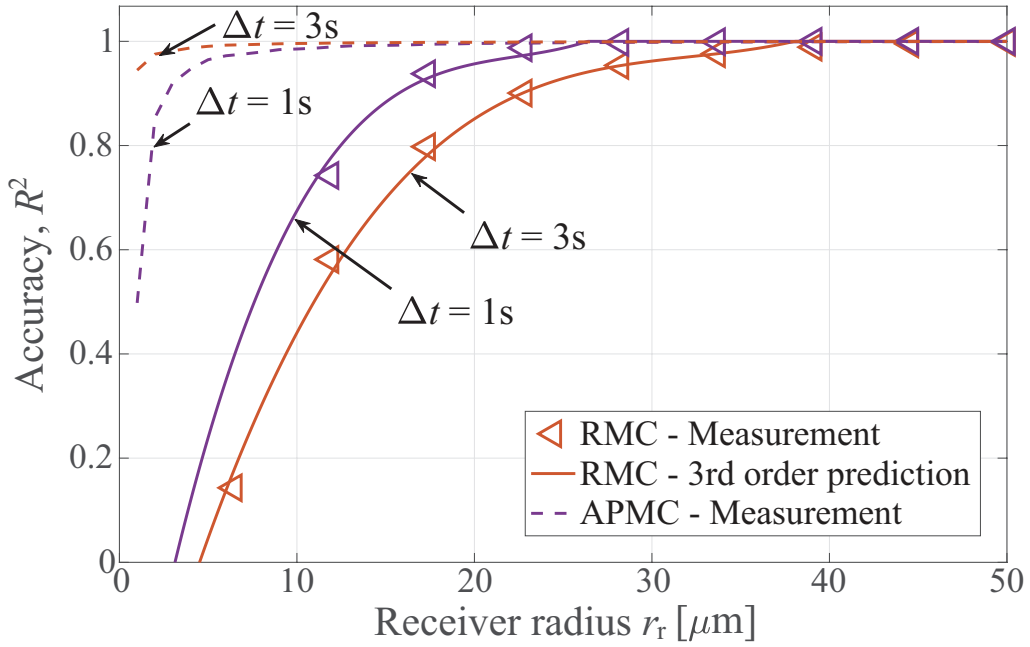

Figure 5.10: Measured and predicted accuracy of the RMC algorithm and the measured accuracy of the APMC algorithm versus r_r for $r_0 = 80\,\mu\mathrm{m}$, $N = 10^6$, $M = 2$, $D = 10^{-9}\,\mathrm{m}^2/\mathrm{s}$, with $\Delta t = 1\,\mathrm{s}$ and $\Delta t = 3\,\mathrm{s}$.

5.4.1 Run time profile

We compare the computational complexity of the APMC algorithm with that of the RMC algorithm. Fig. 5.11 plots the average run time per realization of MATLAB simulation for the APMC and RMC algorithms for $r_0 = 50\,\mu\mathrm{m}$, $N = 10^4$, $D = 10^{-9}\,\mathrm{m}^2/\mathrm{s}$, $r_\mathrm{r} = 20\,\mu\mathrm{m}$, and $\Delta t = 0.01\,\mathrm{s}$, $0.05\,\mathrm{s}$, $0.1\,\mathrm{s}$, $0.5\,\mathrm{s}$, $1\,\mathrm{s}$, $2\,\mathrm{s}$, and $5\,\mathrm{s}$. We clarify that each run time is averaged over at least 20 realizations on an Intel i7 desktop PC.

We first observe from the figure that the averaged run time per realization decreases when Δt becomes higher. This is due to the fact that when Δt increases, the number of simulation time steps in the simulation decreases. This leads to a decrease in the number of propagation and absorption operations, which affects the computational complexity. Second, we observe that the APMC algorithm requires a slightly shorter run time to simulate a system transmission process than the RMC algorithm, except for $\Delta t = 5\,\mathrm{s}$. This is due to the fact that the APMC algorithm absorbs molecules before propagation, saving the computation cost on propagating and tracking will-be-absorbed molecules. When the time step length increases to $\Delta t = 5\,\mathrm{s}$, $\sqrt{D\Delta t}/r_\mathrm{r}$ becomes large and the RMC algorithm leads to a more severe overestimation than the APMC algorithm. Therefore, the RMC algorithm requires a shorter time to simulate than the APMC algorithm.

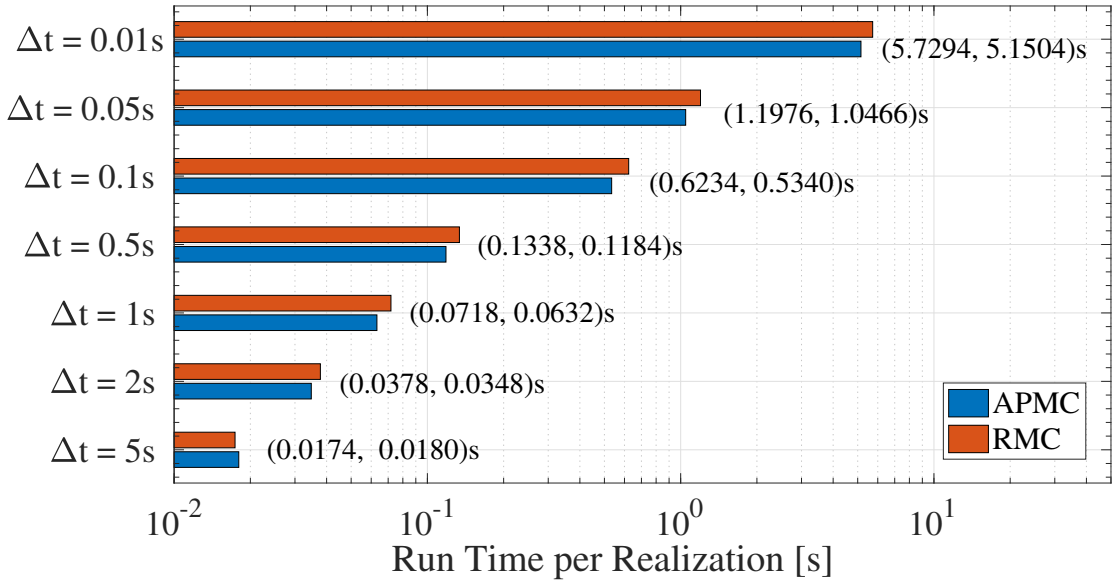

Figure 5.11: Average run time per realization of MATLAB simulation for the APMC and RMC algorithms for $r_0 = 50\,\mu$m, $N = 10^4$, $D = 10^{-9}\,\mathrm{m}^2/\mathrm{s}$, $r_\mathrm{r} = 20\,\mu$m, and $\Delta t = 0.01\,\mathrm{s}$, $0.05\,\mathrm{s}$, $0.1\,\mathrm{s}$, $0.5\,\mathrm{s}$, $1\,\mathrm{s}$, $2\,\mathrm{s}$, and $5\,\mathrm{s}$. Total transmission time is 200 seconds.

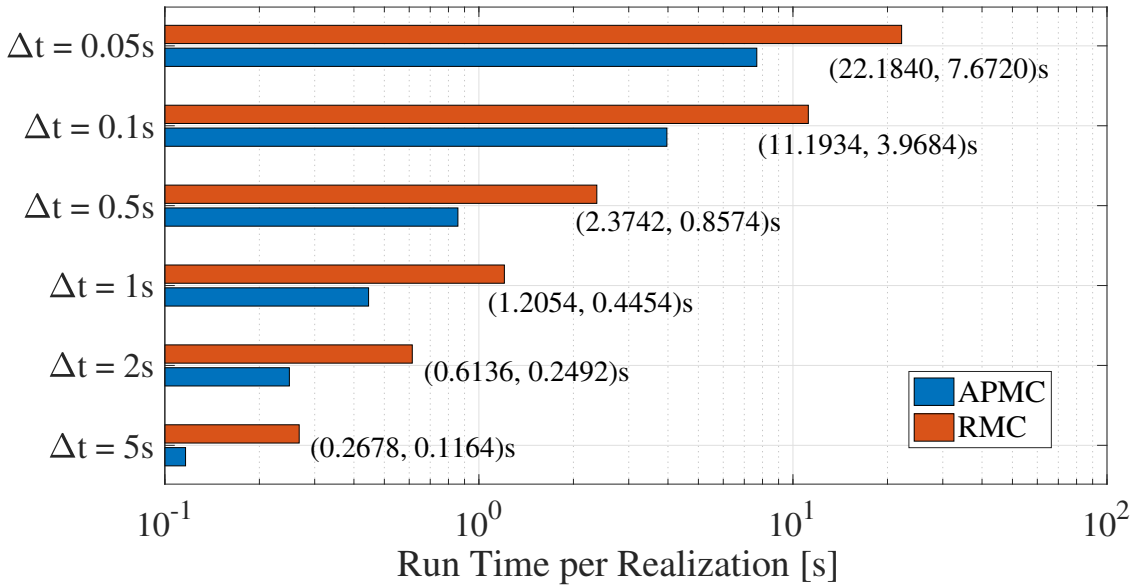

Figure 5.12: Average run time per realization of MATLAB simulation for the APMC and RMC algorithms for $r_0 = 100\,\mu$m, $N = 2 \times 10^3$, $D = 1.05 \times 10^{-9}\,\mathrm{m}^2/\mathrm{s}$, $r_\mathrm{r} = 25\,\mu$m, and $\Delta t = 0.05\,\mathrm{s}$, $0.1\,\mathrm{s}$, $0.5\,\mathrm{s}$, $1\,\mathrm{s}$, $2\,\mathrm{s}$, and $5\,\mathrm{s}$. Total transmission time is 100 seconds.

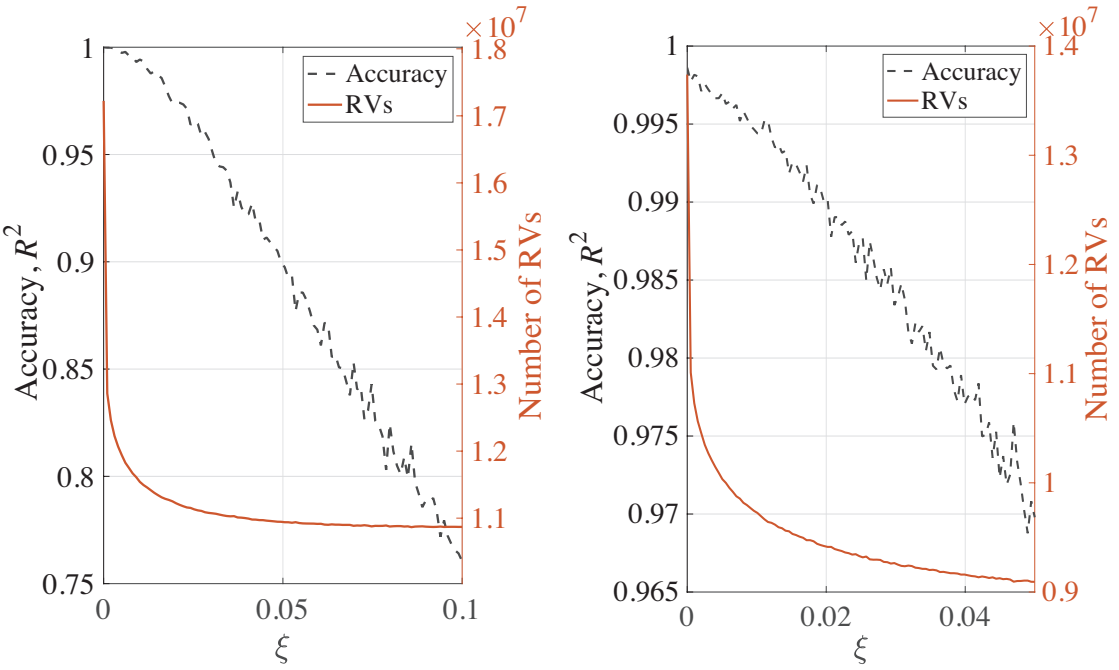

(a) $r_\mathrm{r} = 10\,\mu$m (b) $r_\mathrm{r} = 20\,\mu$m

Figure 5.13: Number of RVs generated and measured accuracy of the APMC algorithm versus ξ for $r_0 = 50\,\mu$m, $M = 10$, $N = 10^6$, $D = 10^{-9}\,\mathrm{m}^2/\mathrm{s}$, $\Delta t = 5\,\mathrm{s}$, and $r_\mathrm{r} = 10\,\mu$m or $r_\mathrm{r} = 20\,\mu$m.

Fig. 5.12 plots the average run time per realization of MATLAB simulation for the APMC and RMC algorithms for two absorbing RXs with $r_0 = 100\,\mu$m, $N = 2 \times 10^3$, $D = 1.05 \times 10^{-9}\,\mathrm{m}^2/\mathrm{s}$, $r_\mathrm{r} = 25\,\mu$m, and $\Delta t = 0.05\,\mathrm{s}$, $0.1\,\mathrm{s}$, $0.5\,\mathrm{s}$, $1\,\mathrm{s}$, $2\,\mathrm{s}$, and $5\,\mathrm{s}$. We clarify that each run time is averaged over at least 20 realizations on an Intel i7 desktop PC. We observe that simulating with the APMC algorithm for two absorbing RXs requires a much shorter run time to complete a system transmission process, less than half of that required by the RMC algorithm. This is again due to the fact that the APMC algorithm absorbs molecules before propagation, saving the computation cost on propagating and tracking will-be-absorbed molecules. As the propagation cost for molecules in a two absorbing RXs system is much larger than that in a single absorbing RX system, the advantage of the APMC algorithm is more obvious in Fig. 5.12 than in Fig. 5.11.

5.4.2 Likelihood threshold application

Figs. 5.13 and 5.14 plot the computational complexity and the measured accuracy of the APMC algorithm and the RMC algorithm, respectively, versus the likelihood threshold ξ for $r_0 = 50\,\mu$m, $M = 10$, $N = 10^6$, and $D = 10^{-9}\,\mathrm{m}^2/\mathrm{s}$. We observe in all subfigures that when ξ increases, the measured accuracy decreases. This is

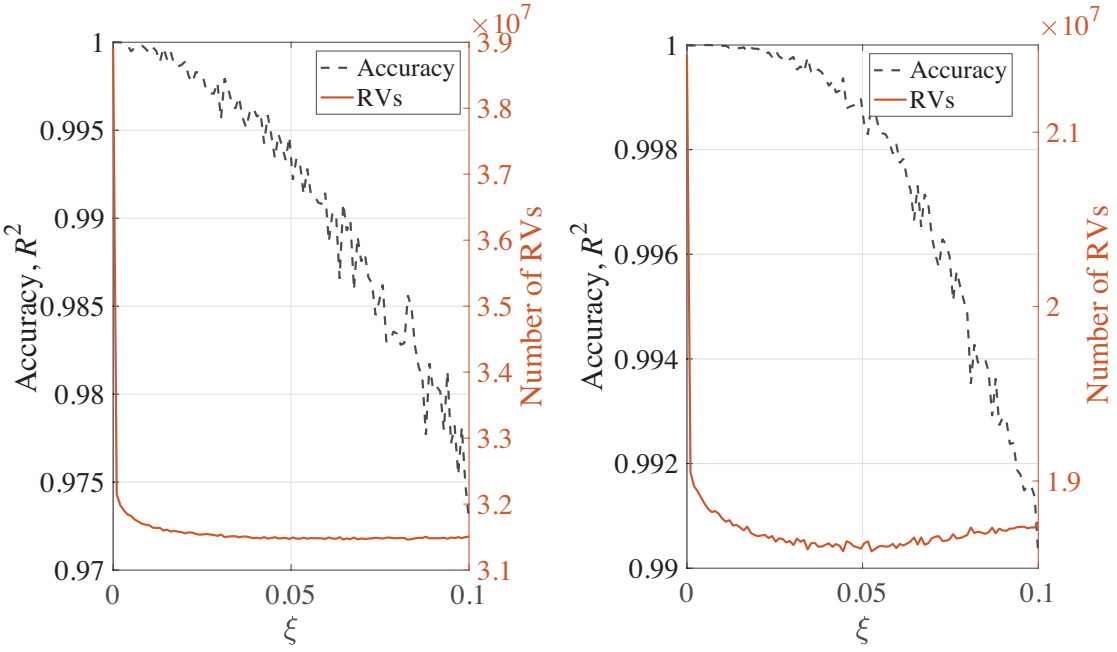

(a) $r_\mathrm{r} = 20\,\mu\mathrm{m}$ (b) $r_\mathrm{r} = 40\,\mu\mathrm{m}$

Figure 5.14: Number of RVs generated and measured accuracy of the RMC algorithm versus ξ for $r_0 = 50\,\mu\mathrm{m}$, $M = 10$, $N = 10^6$, $D = 10^{-9}\,\mathrm{m}^2/\mathrm{s}$, $\Delta t = 0.1\,\mathrm{s}$, and $r_\mathrm{r} = 20\,\mu\mathrm{m}$ or $r_\mathrm{r} = 40\,\mu\mathrm{m}$.

because when a higher likelihood threshold is applied, the number of molecules that have absorption probabilities lower than the threshold increases. We note that ignoring low absorption probabilities leads to an underestimation of the number of absorbed molecules, resulting in lower accuracy. It also leads to a larger number of $\mathcal{N}_\mathrm{g}$ since $\mathcal{N}_\mathrm{g}$ depends on the number of molecules that need to be propagated. We also observe that the growth in $\mathcal{N}_\mathrm{g}$ is negligible compared to the decrease in $\mathcal{N}_\mathrm{u}$ when ξ is low. We further observe in Fig. 5.14(b) that when ξ increases beyond a certain value, the number of generated RVs begins to increase, since the growth in $\mathcal{N}_\mathrm{g}$ eventually outnumbers the reduction in $\mathcal{N}_\mathrm{u}$.

In addition, we observe from Fig. 5.13 and Fig. 5.14 that when r_r increases from $10\,\mu\mathrm{m}$ to $20\,\mu\mathrm{m}$, the change in measured accuracy becomes less severe when applying the same ξ. This is because a larger RX leads to a higher *a priori* absorption probability in the APMC algorithm and a higher intra-step absorption probability in the RMC algorithm. Therefore, the impact of the likelihood threshold on the number of absorptions is smaller for a larger RX. We clarify that Figs. 5.13 and 5.14 reveal the impact of the likelihood threshold on the number of required RVs and the measured accuracy. With the aid of these figures and similar results, a suitable likelihood threshold can be identified to achieve an acceptable loss of accuracy for simulating other system parameters.

Chapter 6

Conclusions and Future Work

This thesis presented several ways to reduce the computational complexity for the simulation of diffusion-based MC systems with absorbing receiver(s). Importantly, a new algorithm named the *a priori* Monte Carlo (APMC) algorithm was proposed to use the *a priori* approach for simulating the fraction of molecules being absorbed by spherical receiver(s). Based on numerical results, it was demonstrated that the APMC algorithm outperforms the existing simulation algorithms for large diffusion step length to receiver radius ratio. The APMC algorithm was shown suitable to be used in simulations for both the single absorbing receiver case and the multiple absorbing receivers case when the diffusion step length is relatively larger than the receiver radius.

Moreover, for the single absorbing receiver case, an expression was proposed to predict the simulation accuracy of an existing algorithm, the refined Monte Carlo (RMC) algorithm, which help to facilitate the choice of simulation time step length. The MATLAB run time profiles of the APMC and RMC algorithms were investigated and likelihood thresholds were applied to the calculated absorption probabilities to reduce the computational complexity of both algorithms. It was revealed that compared to the RMC algorithm, the APMC algorithm significantly reduces the computational complexity of simulating absorbing receivers without compromising accuracy. It was also demonstrated that with an appropriate likelihood threshold, the computational complexities of algorithms can be further reduced with an extremely small loss in accuracy.

To conclude, this thesis provided valuable insights in the reduction in the computational complexity of existing simulation algorithms of diffusion-based MC systems with absorbing receiver(s). In future, extending the APMC algorithm to other reactive surfaces, such as irreversible partially absorbing surface, reversible perfectly absorbing surface, and reversible partially absorbing surface, where the *a priori* probability of surface interaction is obtainable, are promising research directions.

Bibliography

[1] T. Nakano, A. W. Eckford, and T. Haraguchi, *Molecular Communication.* Cambridge, UK: Cambridge University press, 2013.

[2] N. Farsad, H. B. Yilmaz, A. Eckford, C. B. Chae, and W. Guo, "A comprehensive survey of recent advancements in molecular communication," *IEEE Commun. Surv. Tutor.*, vol. 18, no. 3, pp. 1887–1919, thirdquarter 2016.

[3] V. Bluett and N. Green, "Competitive diffusion-influenced reaction of a reactive particle with two static sinks," *J. Phys. Chem. A*, vol. 110, no. 14, pp. 4738–4752, May 2006.

[4] S. S. Andrews and D. Bray, "Stochastic simulation of chemical reactions with spatial resolution and single molecule detail," *Phys. Biol.*, vol. 1, no. 3, p. 137, Aug. 2004.

[5] D. Arifler and D. Arifler, "Monte Carlo analysis of molecule absorption probabilities in diffusion-based nanoscale communication systems with multiple receivers," *IEEE Trans. Nanobiosci.*, vol. 16, no. 3, pp. 157–165, Apr. 2017.

[6] A. Noel, K. C. Cheung, R. Schober, D. Makrakis, and A. Hafid, "Simulating with AcCoRD: Actor-based communication via reaction–diffusion," *Nano Commun. Netw.*, vol. 11, pp. 44–75, Mar. 2017.

[7] T. Suda, M. Moore, T. Nakano, R. Egashira, A. Enomoto, S. Hiyama, and Y. Moritani, "Exploratory research on molecular communication between nanomachines," in *Proc. 2005 GECCO,* Washington, D.C., June 2005, p. 29.

[8] S. Hiyama, Y. Moritani, R. Gojo, S. Takeuchi, and K. Sutoh, "Biomolecular-motor-based autonomous delivery of lipid vesicles as nano-or microscale reactors on a chip," *Lab on a Chip*, vol. 10, no. 20, pp. 2741–2748, Aug. 2010.

[9] H. B. Yilmaz and C.-B. Chae, "Simulation study of molecular communication systems with an absorbing receiver: Modulation and ISI mitigation techniques," *Simulation Model. Practice. Th.*, vol. 49, pp. 136–150, Dec. 2014.

[10] R. B. Bourret and A. M. Stock, "Molecular information processing: lessons from bacterial chemotaxis," *J. Biol. Chem.*, vol. 277, no. 12, pp. 9625–9628, Mar. 2002.

[11] M. S. Kuran, T. Tugcu, and B. O. Edis, "Calcium signaling: Overview and research directions of a molecular communication paradigm," *IEEE Wireless Commun.*, vol. 19, no. 5, pp. 20–27, Oct. 2012.

[12] J. Boedicker and K. Nealson, "Microbial communication via quorum sensing," *IEEE Trans. Mol. Biol. Multi-Scale Commun.*, vol. 1, no. 4, pp. 310–320, Dec. 2015.

[13] S. Balasubramaniam and P. Lio', "Multi-hop conjugation based bacteria nanonetworks," *IEEE Trans. Nanobiosci.*, vol. 12, no. 1, pp. 47–59, Mar. 2013.

[14] C. Villalobos, L. Núñez, and J. García-Sancho, "Anterior pituitary thyrotropes are multifunctional cells," *Am. J. Physiol. Endocrinol. Metab.*, vol. 287, no. 6, pp. e1166–e1170, Dec. 2004.

[15] S. B. Laughlin and T. J. Sejnowski, "Communication in neuronal networks," *Science*, vol. 301, no. 5641, pp. 1870–1874, Sept. 2003.

[16] I. F. Akyildiz, F. Brunetti, and C. Blázquez, "Nanonetworks: A new communication paradigm," *Comput. Netw.*, vol. 52, no. 12, pp. 2260–2279, Aug. 2008.

[17] T. Nakano, T. Suda, Y. Okaie, M. J. Moore, and A. V. Vasilakos, "Molecular communication among biological nanomachines: A layered architecture and research issues," *IEEE Trans. Nanobiosci.*, vol. 13, no. 3, pp. 169–197, Sept. 2014.

[18] C. E. Shannon, "A mathematical theory of communication," *Bell Syst. Tech. J.*, vol. 27, no. 3, pp. 379–423, July 1948.

[19] H. B. Yilmaz and C. Chae, "Arrival modelling for molecular communication via diffusion," *Electron. Lett.*, vol. 50, no. 23, pp. 1667–1669, Nov. 2014.

[20] K. V. Srinivas, A. W. Eckford, and R. S. Adve, "Molecular Communication in fluid media: The additive inverse Gaussian noise channel," *IEEE Trans. Inf. Theory*, vol. 58, no. 7, pp. 4678–4692, July 2012.

[21] H. B. Yilmaz, C.-B. Chae, B. Tepekule, and A. E. Pusane, "Arrival modeling and error analysis for molecular communication via diffusion with drift," in *Proc. 2015 ACM NanoCom,* Boston, MA, Sept. 2015, p. 26.

[22] T. Nakano, T. Suda, M. Moore, R. Egashira, A. Enomoto, and K. Arima, "Molecular communication for nanomachines using intercellular calcium signaling," in *Proc. 2005 IEEE NANO,* Nagoya, Japan, July 2015, pp. 478–481.

[23] M. Moore, A. Enomoto, T. Nakano, R. Egashira, T. Suda, A. Kayasuga, H. Kojima, H. Sakakibara, and K. Oiwa, "A design of a molecular communication system for nanomachines using molecular motors," in *Proc. 2006 IEEE PerCom Workshops,* Pisa, Italy, Mar. 2006, p. 6.

[24] D. Kilinc and O. B. Akan, "Receiver design for molecular communication," *IEEE J. Sel. Areas Commun.*, vol. 31, no. 12, pp. 705–714, Dec. 2013.

[25] T. M. Allen and P. R. Cullis, "Drug delivery systems: Entering the mainstream," *Science*, vol. 303, no. 5665, pp. 1818–1822, Mar. 2004.

[26] A. Ranjan *et al.*, "Nanomedicine for intracellular therapy," *FEMS Microbiol. Lett.*, vol. 332, no. 1, pp. 1–9, June 2012.

[27] L. G. Griffith and G. Naughton, "Tissue engineering–current challenges and expanding opportunities," *Science*, vol. 295, no. 5557, pp. 1009–1014, Feb. 2002.

[28] P. Yager *et al.*, "Microfluidic diagnostic technologies for global public health," *Nature*, vol. 442, no. 7101, pp. 412–418, July 2006.

[29] J. Clausen, "Man, machine and in between," *Nature*, vol. 457, no. 7233, pp. 1080–1081, Feb. 2009.

[30] M. U. Mahfuz, D. Makrakis, and H. T. Mouftah, "On the characterization of binary concentration-encoded molecular communication in nanonetworks," *Nano Commun. Netw.*, vol. 1, no. 4, pp. 289–300, Dec. 2010.

[31] M. S. Kuran, H. B. Yilmaz, T. Tugcu, and I. F. Akyildiz, "Modulation techniques for communication via diffusion in nanonetworks," in *Proc. 2011 IEEE ICC,* Kyoto, Japan, July 2011, pp. 1–5.

[32] M. Ş. Kuran, H. B. Yilmaz, T. Tugcu, and I. F. Akyildiz, "Interference effects on modulation techniques in diffusion-based nanonetworks," *Nano Commun. Netw.*, vol. 3, no. 1, pp. 65–73, Mar. 2012.

[33] N. Garralda, I. Llatser, A. Cabellos-Aparicio, E. Alarcón, and M. Pierobon, "Diffusion-based physical channel identification in molecular nanonetworks," *Nano Commun. Netw.*, vol. 2, no. 4, pp. 196–204, Dec. 2011.

[34] Y.-P. Hsieh, Y.-C. Lee, P.-J. Shih, P.-C. Yeh, and K.-C. Chen, "On the asynchronous information embedding for event-driven systems in molecular communications," *Nano Commun. Netw.*, vol. 4, no. 1, pp. 2–13, Mar. 2013.

[35] B. Tepekule, A. E. Pusane, H. B. Yilmaz, and T. Tugcu, "Energy efficient ISI mitigation for communication via diffusion," in *Proc. 2014 IEEE BlackSeaCom,* Chisinau, Moldova, May 2014, pp. 33–37.

[36] H. Arjmandi, A. Gohari, M. N. Kenari, and F. Bateni, "Diffusion-based nanonetworking: A new modulation technique and performance analysis," *IEEE Commun. Lett.*, vol. 17, no. 4, pp. 645–648, Mar. 2013.

[37] M. Moore, A. Enomoto, T. Nakano, T. Suda, A. Kayasuga, H. Kojima, H. Sakakibara, and K. Oiwa, "Simulation of a molecular motor based communication network," in *Proc. 2006 BIONETICS,* Cavalese, Italy, Dec. 2006, p. 19.

[38] M. S. Kuran, H. B. Yilmaz, and T. Tugcu, "A tunnel-based approach for signal shaping in molecular communication," in *Proc. 2013 IEEE ICC,* Budapest, Hungary, June 2013, pp. 776–781.

[39] L. C. Cobo and I. F. Akyildiz, "Bacteria-based communication in nanonetworks," *Nano Commun. Netw.*, vol. 1, no. 4, pp. 244–256, Dec. 2010.

[40] M. Gregori and I. F. Akyildiz, "A new nanonetwork architecture using flagellated bacteria and catalytic nanomotors," *IEEE J. Sel. Areas Commun.*, vol. 28, no. 4, pp. 612–619, May 2010.

[41] T. Nakano, M. J. Moore, F. Wei, A. V. Vasilakos, and J. Shuai, "Molecular communication and networking: Opportunities and challenges," *IEEE Trans. Nanobiosci.*, vol. 11, no. 2, pp. 135–148, June 2012.

[42] T. Nakano, Y. Okaie, and J. Liu, "Channel model and capacity analysis of molecular communication with Brownian motion," *IEEE Commun. Lett.*, vol. 16, no. 6, pp. 797–800, June 2012.

[43] H. B. Yilmaz, A. C. Heren, T. Tugcu, and C. B. Chae, "Three-dimensional channel characteristics for molecular communications with an absorbing receiver," *IEEE Commun. Lett.*, vol. 18, no. 6, pp. 929–932, June 2014.

[44] Y. Deng, A. Noel, M. Elkashlan, A. Nallanathan, and K. C. Cheung, "Modeling and simulation of molecular communication systems with a reversible adsorption receiver," *IEEE Trans. Mol. Biol. Multi-Scale Commun.*, vol. 1, no. 4, pp. 347–362, Dec. 2015.

[45] R. Phillips, J. Theriot, J. Kondev, and H. Garcia, *Physical biology of the cell*. New York, NJ: Garland Science, 2012.

[46] R. Lentini, S. P. Santero, F. Chizzolini, D. Cecchi, J. Fontana, M. Marchioretto, C. Del Bianco, J. L. Terrell, A. C. Spencer, L. Martini *et al.*, "Integrating artificial with natural cells to translate chemical messages that direct E. coli behaviour," *Nat. Comm.*, vol. 5, p. 4012, May 2014.

[47] M. E. Ortiz and D. Endy, "Engineered cell-cell communication via DNA messaging," *J. Biol. Eng.*, vol. 6, no. 1, pp. 16–17, Dec. 2012.

[48] N. Farsad, W. Guo, and A. W. Eckford, "Tabletop molecular communication: Text messages through chemical signals," *PLoS ONE*, vol. 8, no. 12, p. e82935, Dec. 2013.

[49] COMSOL Inc. COMSOL Multiphysics. [Online]. Available: http://www.comsol.com

[50] ANSYS Inc. ANSYS. [Online]. Available: http://www.ansys.com

[51] S. S. Andrews, N. J. Addy, R. Brent, and A. P. Arkin, "Detailed simulations of cell biology with Smoldyn 2.1," *PLoS Comput. Biol.*, vol. 6, no. 3, p. e1000705, Mar. 2010.

[52] J. S. van Zon and P. R. Ten Wolde, "Simulating biochemical networks at the particle level and in time and space: Green's function reaction dynamics," *Phys. Rev. Lett.*, vol. 94, no. 12, p. 128103, Apr. 2005.

[53] G. Wei, P. Bogdan, and R. Marculescu, "Efficient modeling and simulation of bacteria-based nanonetworks with BNSim," *IEEE J. Sel. Areas Commun.*, vol. 31, no. 12, pp. 868–878, Dec. 2013.

[54] L. Felicetti, M. Femminella, and G. Reali, "Simulation of molecular signaling in blood vessels: Software design and application to atherogenesis," *Nano Commun. Netw.*, vol. 4, no. 3, pp. 98–119, Sept. 2013.

[55] I. Llatser, D. Demiray, A. Cabellos-Aparicio, D. T. Altilar, and E. Alarcón, "N3sim: Simulation framework for diffusion-based molecular communication nanonetworks," *Simulation Model. Practice. Th.*, vol. 42, pp. 210–222, Mar. 2014.

[56] Y. Jian, B. Krishnaswamy, C. M. Austin, A. O. Bicen, J. E. Perdomo, S. C. Patel, I. F. Akyildiz, C. R. Forest, and R. Sivakumar, "NanoNS3: Simulating

bacterial molecular communication based nanonetworks in Network Simulator 3," in *Proc. 2016 ACM NanoCom,* New York, NJ, Sept. 2016, p. 17.

[57] A. Hellander, S. Hellander, and P. Lotstedt, "Coupled mesoscopic and microscopic simulation of stochastic reaction-diffusion processes in mixed dimensions," *Multi-scale Model. Sim.*, vol. 10, no. 2, pp. 585–611, May 2012.

[58] K. Schulten and I. Kosztin, "Lectures in theoretical biophysics," *University of Illinois*, 2000.

[59] P. M. Morse and H. Feshbach, "Methods of theoretical physics," *Am. J. Phys.*, vol. 22, no. 6, pp. 410–413, Sept. 1954.

[60] ——, *Methods of Theoretical Physics, Part I: International Series in Pure and Applied Physics.* New York, NY: McGraw-Hill, 1953.

[61] R. D. Stoy, "Solution procedure for the Laplace equation in bispherical coordinates for two spheres in a uniform external field: Perpendicular orientation," *J. Appl. Phys.*, vol. 66, no. 10, pp. 5093–5095, Aug. 1989.

[62] T. Dunster, "Legendre and related functions," in *NIST Handbook of Mathematical Functions Hardback and CD-ROM.* Cambridge, UK: Cambridge University press, 2010, pp. 351–381.

[63] J. Crank, *The Mathematics of Diffusion.* Oxford, UK: Oxford University Press, 1979.

[64] G. Marsaglia and T. A. Bray, "A convenient method for generating normal variables," *SIAM Rev.*, vol. 6, no. 3, pp. 260–264, July 1964.